Pure Appl. Chem., Vol. 82, No. 5, pp. 1065–1097, 2010.
doi:10.1351/PAC-REP-09-10-24
© 2010 IUPAC, Publication date (Web): 20 April 2010

Empirical and theoretical models of equilibrium and non-equilibrium transition temperatures of supplemented phase diagrams in aqueous systems (IUPAC Technical Report)*

Horacio R. Corti[1,‡], C. Austen Angell[2], Tony Auffret[3], Harry Levine[4], M. Pilar Buera[1], David S. Reid[5], Yrjö H. Roos[6], and Louise Slade[4]

[1]Faculty of Exact and Natural Sciences, University of Buenos Aires, Int. Cantilo s/n. Pabellón II Ciudad Universitaria, Buenos Aires, Argentina; [2]Department of Chemistry, Arizona State University, Tempe, AZ 85287, USA; [3]Global Research & Development, Pfizer, Ltd., Ramsgate Road, Sandwich, Kent CT13 9NJ, UK; [4]Food Polymer Science Consultancy, Morris Plains, NJ 07950, USA; [5]Department of Food Science and Technology, University of California at Davis, 1 Shields Ave., Davis, CA 95616-8571, USA; [6]Department of Food and Nutritional Sciences, University College, Cork, Ireland

Abstract: This paper describes the main thermodynamic concepts related to the construction of supplemented phase (or state) diagrams (SPDs) for aqueous solutions containing vitrifying agents used in the cryo- and dehydro-preservation of natural (foods, seeds, etc.) and synthetic (pharmaceuticals) products. It also reviews the empirical and theoretical equations employed to predict equilibrium transitions (ice freezing, solute solubility) and non-equilibrium transitions (glass transition and the extrapolated freezing curve). The comparison with experimental results is restricted to carbohydrate aqueous solutions, because these are the most widely used cryoprotectant agents. The paper identifies the best standard procedure to determine the glass transition curve over the entire water-content scale, and how to determine the temperature and concentration of the maximally freeze-concentrated solution.

Keywords: aqueous solutions; carbohydrates; cryoprotectants; freezing point; glass transition; IUPAC Physical and Biophysical Chemistry Division; maximally freeze-concentrated solution; solubility; state phase diagrams.

CONTENTS

1. INTRODUCTION
2. THERMODYNAMICS OF THE EQUILIBRIUM-PHASE TRANSITIONS
   - 2.1 Freezing transition curve
   - 2.2 Solute solubility curve
   - 2.3 Theoretical models for the excess Gibbs energy of solution

*Sponsoring body: IUPAC Physical and Biophysical Chemistry Division: see more details on p. 1093.

‡Corresponding author: E-mail: hrcorti@cnea.gov.ar

3. THEORETICAL MODELS FOR PREDICTING NON-EQUILIBRIUM-PHASE TRANSITIONS IN AQUEOUS SYSTEMS
   3.1 Glass transition models
   3.2 Prediction of the maximally freeze-concentrated point
4. RESULTS
   4.1 Freezing point and carbohydrate solubility in aqueous solutions
   4.2 Glass transition temperature
   4.3 Maximally freeze-concentrated point
5. MOLECULAR DYNAMICS SIMULATIONS OF THE GLASS TRANSITION
6. CONCLUSIONS AND OUTLOOK
MEMBERSHIP OF SPONSORING BODIES
ACKNOWLEDGMENTS
REFERENCES

1. INTRODUCTION

The supplemented phase diagram (SPD) of a simple binary aqueous system is a combination of equilibrium-phase transition curves, representing the phase diagram, and non-equilibrium-phase/state transition curves, as shown in Fig. 1. The phase diagram describes thermodynamic behavior, and as such requires a demonstration of equilibrium. It defines the final resting points, route-independent, of the system under a range of applied conditions. The equilibrium curves are the freezing curve, which describes the temperature dependence of the concentration of the unfrozen phase in contact with ice, and the solubility curve, representing the temperature dependence of the solute saturation concentration. Both curves merge at the eutectic, at temperature T_E and concentration w_E.

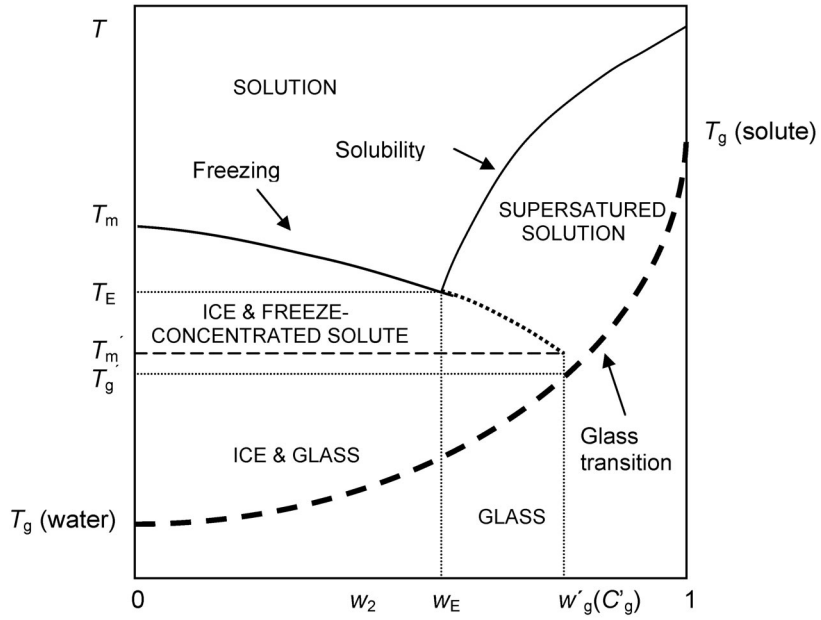

Fig. 1 Scheme of the SPD, temperature vs. mass fraction of solute of a binary aqueous system.

The state diagram also describes the phases in the system. However, it does not imply equilibrium, but describes the phases potentially present under different conditions after following some particular protocol. While this diagram still illustrates the phase relationships as a function of temperature and composition, the locations of the boundaries are route- and time-dependent.

The glass transition (T_g) curve in the SPD represents the temperatures at which, for a given composition, the mechanical relaxation time becomes comparable with the time scale for the experiment, that is, of the order of 100 s. It is clearly a route-dependent curve whose location depends on the technique used to determine it, and even the use of a single technique could lead to different T_g values.

If a solute fails to crystallize when the eutectic composition is reached, cooling will result in further ice formation and the locus of solute concentration in the remaining unfrozen phase will extend beyond the equilibrium curve (dotted line in Fig. 1). There is a temperature, T_m', at which the unfrozen phase reaches the solute concentration of the maximally freeze-concentrated matrix, w_g', usually designated as $C_g' = 100\ w_g'$ in the literature. Below that temperature, the unfrozen phase will vitrify with no further changes in concentration. This unfrozen phase will show a glass transition with the glass transition temperature of the maximally freeze-concentrated matrix, T_g' [1–5].

Kinetic constraints may reduce the amount of ice formed, so the dotted line in Fig. 1 represents a limiting case. If the rate of cooling exceeds the maximum achievable rate of crystallization, then the unfrozen phase will be more dilute than the maximally freeze-concentrated phase, which represents the only metastable state unambiguously defined.

During rewarming a cryoconcentrated system, the observed thermal transitions are the glass transition of the freeze-concentrated solution (T_g), the formation of ice (devitrification), and the melting of the ice (T_m). The T_g of the freeze-concentrated solution approaches T_g' when the system approaches maximum cryoconcentration, which can be attained by a sufficiently slow freezing rate, enough time at the adequate temperature for ice formation and/or by cooling–rewarming cycles within the adequate temperature range. Roos and Karel [6,7] found that the onset temperatures of ice melting (T_m') in the maximally freeze-concentrated solutions could approach the T_g' values for a polymer such as starch at a relatively high temperature. However, for some sugars such as sucrose, the glass transition is almost complete below T_m' and the gap between T_g' and T_m' is increased.

Different experimental techniques have been used in determining phase/state diagrams, such as conventional or modulated differential scanning calorimetry (DSC), dielectric thermal analysis (DETA), dynamic mechanical thermal analysis (DMTA), and thermally stimulated current (TSC), based on thermal, dielectric, mechanical and electrical relaxations, respectively. Moreover, volume expansion (dilatometry) and molecular relaxation or mobility, sensed by different methods of spectroscopy (NMR, ESR), can be used to determine thermal transitions.

These techniques have practical limitations [8], which will not be addressed here, but in a forthcoming Technical Report. Most of the problems associated with the determination of thermal transitions are due to the effectiveness of the coupling between sample and measuring sensor, the sample size, scanning rate, or frequency. However, if the test conditions are properly chosen, different techniques gave slightly different temperature values for the glass transition, crystallization, and melting [9].

The key question we want to address here has been recently formulated by one of us [8] from the point of view of the meaning of different experimental techniques: How do we locate the boundaries within our state diagrams and what might they represent? In this report, we will discuss how we can assess those boundaries using empirical or theoretical models when the experimental information is not available or is incomplete. We will emphasize the prediction of transition temperatures to construct SPDs in aqueous systems because of their relevance in cryopreservation.

2. THERMODYNAMICS OF THE EQUILIBRIUM-PHASE TRANSITIONS

The classical solution thermodynamic formulation of the freezing temperature of water (ice melting) as a function of the solute concentration and the temperature dependence of the solute solubility is pre-

sented in this section. Subscripts 1, 2, and 3 refer to solvent (water), anhydrous solute, and hydrated solute, respectively.

In the thermodynamic formulation within this section, we will use different conventions for the activity coefficient and solute composition scales. Thus, the symmetrical convention takes the pure liquid at the temperature and pressure of the system as the hypothetical reference state, while the asymmetrical convention uses the pure liquid reference state for the solvent (water) and infinite dilution for the solute.

2.1 Freezing transition curve

The freezing point depression by adding a solute is one of the most important methods of determining activity coefficients or osmotic coefficients of solutions. Here we describe the equivalent thermodynamic problem of calculating freezing point depression of an aqueous solution containing a known concentration of solute.

We take the pure liquid water as the standard state of unit activity and assuming chemical equilibrium between water in the solution and ice

$$\mu_1^\circ(\mathrm{s}) = \mu_1^\circ(\mathrm{l}) + RT \ln a_1 \tag{1}$$

we obtain the well-known expression [10]

$$\left(\frac{\partial \ln a_1}{\partial T}\right)_p = \frac{\Delta_{\mathrm{fus}} H_{\mathrm{m},1}}{RT^2} \tag{2}$$

where a_1 is the water activity (equal to the ice activity at the equilibrium temperature), and $\Delta_{\mathrm{fus}}H_{\mathrm{m},1}$ is the molar fusion (melting) enthalpy of pure water at the equilibrium temperature and at the standard pressure of 0.1 MPa. The classical treatment [10] assumes that the difference in the molar heat capacities of liquid water and ice, $\Delta C_{p,\mathrm{m},1}$, is temperature-independent and

$$\Delta_{\mathrm{fus}} H_{\mathrm{m},1} = \Delta_{\mathrm{fus}} H_{\mathrm{m},1}{}^\circ - \left(T_1{}^\circ - T\right) \Delta C_{p,\mathrm{m},1}{}^\circ \tag{3}$$

where $T_1{}^\circ$ = 273.15 K is the fusion temperature of pure water, $\Delta_{\mathrm{fus}}H_{\mathrm{m},1}{}^\circ$ = 6002 J mol^{-1} [17] is the melting enthalpy of pure water at $T_1{}^\circ$, and $\Delta C_{p,\mathrm{m},1}{}^\circ$ = 38.03 J mol^{-1} K^{-1} [17] is the difference in the molar heat capacities of liquid water and ice at $T_1{}^\circ$, assumed to be independent of temperature. All these values correspond to the standard pressure $p^\ominus$ = 0.1 MPa. After replacing eq. 3 in eq. 2 and integration, one has

$$\ln a_1 = \ln\left(f_1 x_1\right) = \frac{\Delta_{\mathrm{fus}} H_{\mathrm{m},1}{}^\circ}{R}\left(\frac{1}{T_1{}^\circ} - \frac{1}{T}\right) - \frac{\Delta C_{p,\mathrm{m},1}{}^\circ}{R}\left(\ln\frac{T_1{}^\circ}{T} + 1 - \frac{T_1{}^\circ}{T}\right) \tag{4}$$

where x_1 is the water mole fraction, f_1 is the water activity coefficient in the mole fraction scale. The freezing point of the aqueous solution can be obtained by solving eq. 4 iteratively, provided that the osmotic coefficient of the solution, ϕ, related to the water activity by

$$\ln a_1 = -M_1 \phi \sum_i m_i \tag{5}$$

is known as a function of temperature and the total molality, $m = \Sigma\, m_i$ of all the solute species, M_1 being the water molar mass. In Section 3, we will review the models to obtain the water activity or the osmotic coefficient of the solution.

The approximation $\Delta C_{p,\mathrm{m},1} = \Delta C_{p,\mathrm{m},1}{}^\circ$ can be avoided by resorting to the experimental information on the heat capacity of ice [11] and supercooled water [12,13], as proposed by Spencer et al. [14].

Thus, the difference of standard chemical potentials of ice and water was fitted to the data reported by Speedy [13] down to –46 °C, using the equation

$$\frac{\mu_1(\mathrm{s})^\circ - \mu_1(\mathrm{l})^\circ}{RT} = c_1 + c_2 T + c_3 T^2 + c_4 T^3 + \frac{c_5}{T} + c_6 \ln T \tag{6}$$

where c_1 = 7875.060 393, c_2 = 11.691 184 90 K^{-1}, c_3 = –0.017 183 789 K^{-2}, c_4 = 1.243 955 43 10^{-5} K^{-3}, c_5 = –93 314.790 K, c_6 = –1728.7461 [14].

The freezing temperature can be obtained by iterative solution of eqs. 1, 4, and 6 and the experimental data for the osmotic coefficient of the solution described, for instance, with the models reviewed in Section 3.1. The validity of this approach extends between 0 °C, the melting point of pure water, and –50 °C, which is suitable for most of the polyol-water systems of interest in practical cryopreservation.

2.2 Solute solubility curve

The most general case to consider is that where an anhydrous solute forms a hydrate with n_h water molecules at the transition temperature, T_t, corresponding to the hydration equilibrium

$$\mathrm{S\ (aq)} + n_h\ \mathrm{H_2O} \leftrightarrows \mathrm{S{\cdot}}n_h\mathrm{H_2O\ (s)}$$

where n_h is the hydration number. If T is higher than T_t, or if no hydrated form exists, the solute crystallizes in the anhydrous form and its solubility can be determined from the solute molar enthalpy of fusion, $\Delta_{fus}H_{m,2}$, at the melting temperature [15]

$$\ln(x_2 f_2) = -\frac{\Delta_{fus}H_{m,2}(T_2^\circ)}{R}\left(\frac{1}{T} - \frac{1}{T_2^\circ}\right) + \frac{\Delta_{fus}C_{p,m,2}}{R}\ln\left(\frac{T}{T_2^\circ}\right) + \frac{\Delta_{fus}C_{p,m,2}}{R}T_2^\circ\left(\frac{1}{T} - \frac{1}{T_2^\circ}\right) \tag{7}$$

where f_2 is the symmetrical activity coefficient of the solute in the mole fraction scale, T_2° is the melting temperature of the pure solute, $\Delta_{fus}C_{p,m,2}$ is the difference in the solute heat capacities in the pure liquid and in the pure solid state, which it is assumed independent of temperature in eq. 7. In case that $\Delta_{fus}C_{p,m,2}$ could be considered as a linear function of temperature between T and T_2°, that is, $\Delta_{fus}C_{p,m,2} = A + B\,(T - T^\circ)$, the expression for the solute activity becomes

$$\begin{aligned}\ln(x_2 f_2) = &\left[-\frac{\Delta_{fus}H_{m,2}(T_2^\circ)}{R} + \frac{A - BT^\circ}{R}T_2^\circ + \frac{B}{2R}(T_2^\circ)^2\right]\left(\frac{1}{T} - \frac{1}{T_2^\circ}\right) + \\ &\frac{A - BT^\circ}{R}\ln\left(\frac{T}{T_2^\circ}\right) + \frac{B}{2R}(T - T_2^\circ)\end{aligned} \tag{8}$$

If T is lower than T_t, the hydrated solute crystallizes and the chemical potential equilibrium condition $\mu_3(\mathrm{s}) = \mu_2(\mathrm{aq}) + n_h\mu_1(\mathrm{aq})$, leads to [16]

$$\begin{aligned}n_h \ln(x_1 f_1) + \ln(x_2 f_2) = &-\frac{\Delta_{fus}H_{m,3}(T_3^\circ)}{R}\left(\frac{1}{T} - \frac{1}{T_3^\circ}\right) + \frac{\Delta_{fus}C_{p,m,3}}{R}\ln\left(\frac{T}{T_3^\circ}\right) + \\ &\frac{\Delta_{fus}C_{p,m,3}}{R}T_3^\circ\left(\frac{1}{T} - \frac{1}{T_3^\circ}\right) + n_h \ln\left[\frac{n_h}{n_h + 1}f_1(T_3^\circ)\right] + \ln\left[\frac{1}{n_h + 1}f_2(T_3^\circ)\right]\end{aligned} \tag{9}$$

where f_1 is the symmetrical activity coefficient of water in the mole fraction scale, T_3° is the melting temperature of the hydrated solute, $\Delta_{fus}C_{p,m,3}$ is the difference in the hydrated solute heat capacities in the pure liquid and in the pure solid state, at T° = 298.15 K.

The solute solubility of the anhydrous solute can be calculated iteratively with eq. 8, provided that the enthalpy of fusion, the melting point, and the heat capacities (liquid and solid) of the solute are known, along with the experimental data for the activity coefficient of the solute described with the models reviewed in Section 3.1. In the case of a hydrated solute, the solubility calculation by using eq. 9 requires the knowledge of thermodynamic properties of the hydrate and additional information, such as the hydration number, n_h, and the pure liquid enthalpy and heat capacity of water.

Alternatively, the asymmetrical convention can be used [17], and replacing the enthalpy of fusion by the enthalpy of dilution, the following expression is obtained for the anhydrous solute:

$$\ln\left(x_2 f_2 *\right) = -\frac{\Delta_{\mathrm{dil}} H_{\mathrm{m},2}\left(T_2{}^\circ\right)}{R}\left(\frac{1}{T}-\frac{1}{T_2{}^\circ}\right)+\frac{\Delta_{\mathrm{dil}} C_{p,\mathrm{m},2}}{R}\left[\ln\left(\frac{T}{T_2{}^\circ}\right)+\left(\frac{T_2{}^\circ}{T}-1\right)\right]- \ln\left(f_2^{\infty}\left(T_2{}^\circ\right)\right) \tag{10}$$

where f_2* is the asymmetrical activity coefficient of the solute in the mole fraction scale (f_2* = $f_2/f_2{}^\infty$), $f_2{}^\infty$ being the activity coefficient of the solute at infinite dilution in the symmetrical convention. The molar enthalpy of dilution, $\Delta_{\mathrm{dil}}H_{\mathrm{m},2}$, is the difference between the molar enthalpy of the solution at infinite dilution and the molar enthalpy of the pure solid, and $\Delta_{\mathrm{dil}}C_{p,\mathrm{m},2} = C_{p,\mathrm{m},2}{}^\infty - C_{p,\mathrm{m},2}{}^\circ(\mathrm{s})$.

For the hydrated form

$$n_h \ln\left(x_1 f_1\right) + \ln\left(x_2 f_2 *\right) = -\frac{\Delta_{\mathrm{dil}} H_{\mathrm{m},3}\left(T_3{}^\circ\right)}{R}\left(\frac{1}{T}-\frac{1}{T_3{}^\circ}\right)+\frac{\Delta_{\mathrm{dil}} C_{p,\mathrm{m},3}}{R}\ln\left(\frac{T}{T_3{}^\circ}\right)+ \frac{\Delta_{\mathrm{dil}} C_{p,\mathrm{m},3}}{R} T_3{}^\circ\left(\frac{1}{T}-\frac{1}{T_3{}^\circ}\right)+ n_h \ln\left[\frac{n_h}{n_h+1} f_1\left(T_3{}^\circ\right)\right]+\ln\left[\frac{1}{n_h+1} f_2 *\left(T_3{}^\circ\right)\right] \tag{11}$$

where $\Delta_{\mathrm{dil}}C_{p,\mathrm{m},3} = C_{p,\mathrm{m},2}{}^\infty + n_h C_{p,\mathrm{m},1}{}^\circ(\mathrm{l}) - C_{p,\mathrm{m},3}{}^\circ(\mathrm{s})$, and $\Delta_{\mathrm{dil}}H_{\mathrm{m},3}\,(T_3{}^\circ) = \Delta_{\mathrm{dil}}H_{\mathrm{m},3}\,(T^\circ) + \Delta_{\mathrm{dil}}C_{p,\mathrm{m},3}\,(T_3{}^\circ - T^\circ)$.*

Jónsdóttir et al. [16] quoted that the asymmetrical expression leads to higher values of error because the activity coefficients at infinite dilution are more difficult to determine and the enthalpy of dilution is normally measured at T° and need to be calculated at the melting temperature of the solute.

2.3 Theoretical models for the excess Gibbs energy of solution

As shown in the previous sections, the freezing and solubility equilibrium curves can be predicted by standard thermodynamic methods if the activity coefficient (alternatively, the osmotic coefficient) of the solute in the solution is known as a function of temperature and composition [18], along with enthalpy and heat capacity changes on dissolution or melting. Also, the effect of pressure on the equilibrium curves can be estimated if the partial molar volume of the solute in the aqueous solution is known.

The key thermodynamic quantity to predict osmotic or activity coefficients in solution is the molar excess Gibbs energy function, $G_{\mathrm{m}}{}^{\mathrm{E}}$, defined as the difference between the molar Gibbs energy of mixture and the ideal mixture molar Gibbs energy

$$G_{\mathrm{m}}^{\mathrm{E}} = \Delta_{\mathrm{mix}} G_{\mathrm{m}} - RT\sum_i x_i \ln x_i = RT\sum_i x_i \ln f_i \tag{12}$$

*The equations for the solubility of anhydrous and hydrated solutes within this subsection were expressed in the form quoted in the original references, except for changes in nomenclature to adjust them to the IUPAC recommendations. A rigorous thermodynamics formalism for solid + liquid systems with compound (hydrate) formation can be found in a recent IUPAC Technical Report "The IUPAC-NIST Solubility Data Series: A guide to preparation and use of compilations and evaluations", Analytical Chemistry Division, Subcommittee on Solubility and Equilibrium Data.

© 2010, IUPAC

where $\Delta_{mix}G_m$ is the molar Gibbs energy of mixture and x_i represents the mole fraction of the component *i*. For a binary solution at constant temperature and pressure, the Gibbs–Duhem relationship leads to

$$RT \ln f_1 = G_m^E - x_2 \frac{\partial G_m^E}{\partial x_2} \tag{13}$$

$$RT \ln f_2 = G_m^E - (1 - x_2) \frac{\partial G_m^E}{\partial x_2} \tag{14}$$

All the models developed to predict thermodynamic properties of mixtures start by proposing an expression for $G_m{}^E$, as we will see in the following sections.

Modified UNIQUAC model

The UNIQUAC model [19] describes properly the temperature dependence of $G_m{}^E$ for suitable calculation of the activity coefficient of water, and it was used by Le Maguer [20] with revised structural parameters by the building block method to correlate $G_m{}^E$ and $H_m{}^E$ of aqueous carbohydrates. However, Catté et al. [17] pointed out that more robust expressions must be used to obtain precise predictions of solute solubility by temperature derivations. They used the modified UNIQUAC model, proposed by Larsen et al. [21] who calculate $G_m{}^E$ as the sum

$$\frac{G_m^E}{RT} = \sum_i x_i \ln\left(\frac{\omega_i}{x_i}\right) - \sum_i q_i x_i \ln\left(\sum_j \theta_j \tau_{ji}\right) \tag{15}$$

where the first term on the right side of eq. 15 is the combinatorial term, ω_i being the volume fraction of the component *i*, given by

$$\omega_i = \frac{x_i r_i^{2/3}}{\sum_j x_j r_j^{2/3}} \tag{16}$$

r_i being the molecular volume parameter of component *i.*

The residual contribution (second term on the right side of eq. 15) contains the molecular surface area parameter, q_i, and the surface area fraction, θ_i, given by

$$\theta_i = \frac{q_i x_i}{\sum_j q_j x_j} \tag{17}$$

Both adimensional parameters, r_i and q_i, are calculated as the sum of the group volumes R_k and group surface areas Q_k, respectively

$$r_i = \sum_k \nu_{k,i} R_k \qquad q_i = \sum_k \nu_{k,i} Q_k \tag{18}$$

where $\nu_{k,i}$ is the number of groups of type *k* in molecule *i*. Group parameters R_k and Q_k are obtained from the van der Waals group volumes and surfaces, respectively, given by Bondi [22].

© 2010, IUPAC

The Boltzmann factors, τ_{ij}, are related to the temperature-dependent interaction parameters, a_{ij}, as

$$\tau_{ij} = \exp\left(-\frac{a_{ij}(T)}{T}\right) = \exp\left(-\frac{u_{ij} - u_{ii}}{RT}\right) \tag{19}$$

where $a_{ij}(T/\mathrm{K}) = a_{ij1}/\mathrm{K} + a_{ij2}(T/K - T^\circ) + a_{ij3}[(T/\mathrm{K})\ \ln(T^\circ/T) + T/\mathrm{K} - T^\circ]$, with $T^\circ = 298.15$ K, is related to the difference between the interaction potential of the pair of molecules i and j and the interaction of the $i - i$ pair [21].

Thus, for a binary aqueous solution, the modified UNIQUAC model requires the knowledge of the parameters r_i, q_i, for the pure components and six (a_{ws1}, a_{ws2}, a_{ws3}) interaction coefficients for the water-solute pair. Catté et al. [17] summarized these coefficients for glucose, fructose, and sucrose in water (see Table 1), estimated from experimental data (water activity, osmotic coefficient, excess Gibbs energy, excess enthalpy, boiling temperature, freezing temperature, solubility of anhydrous sugar) on binary water + sugar systems.

Table 1 UNIQUAC parameters for water + sugar mixtures. First-row parameters from ref. [17], second-row parameters from ref. [23].

Component	r_i	q_i	a_{ws1}/K	a_{ws2}	a_{ws3}	a_{sw1}/K	a_{sw2}	a_{sw3}
Water	0.9200	1.40	–	–	–	–	–	–
D-Glucose	8.1528	8.102	26.2775	–1.4567	–2.5222	–5.6142	1.7631	–0.5151
	8.1528	7.920	96.5267	0.2770	–	–68.6157	–0.0690	–
D-Fructose	8.1529	8.186	17.4626	–1.7294	–2.7505	0.8591	2.0314	–0.4329
	8.1529	8.004	42.3676	–2.2511	–	–28.2892	1.7780	–
Sucrose	14.5496	14.310	92.6880	–0.5538	0.5935	–69.6757	0.5589	–0.7496
	14.5496	13.764	118.995	–0.3410	–	–89.3391	0.3280	–

Peres and Macedo [23] proposed to reduce the number of interaction parameters in the modified UNIQUAC model by using a linear temperature dependence, $a_{ij}(T) = a_{ij1} + a_{ij2}(T - T^\circ)$, for the interaction parameters. They used the symmetric convention for the activity coefficients, that is, the standard state for the solute is the pure liquid at the solution temperature, instead of infinite dilution. Thus, the model can be used to predict solubility in mixed solvent mixtures [24]. The interaction parameters estimated from experimental data for binary water + sugar systems (water activity, osmotic coefficient, vapor pressure, boiling temperature, freezing temperature, solubility of anhydrous sugar) are tabulated in Table 1.

Jónsdóttir et al. [16] proposed the use of the original UNIQUAC model [19] to calculate solid + liquid equilibria in saccharides aqueous solutions, with the interaction parameters a_{ws} and a_{sw}, describing the interaction sugar–water, calculated with molecular mechanics methods. The model, named TIEC (theoretical interaction energy calculations), has no adjustable parameters since the interaction parameters calculated for the water + 1,2-ethanediol mixture were used for all the systems analyzed.

The root mean square deviations (RMSDs) and the absolute average deviations, calculated from the experimental and predicted values of the freezing point and the sugar solubility, using both sets of parameters indicated that the four-parameter UNIQUAC model [23] yields better predictions than the six-parameter one. For instance, RMSDs for the freezing point of glucose, fructose, and sucrose are 1.80, 3.22, and 1.76 %, respectively, calculated with the six-parameter model, but decrease to 0.90, 1.83, and 1.44 %, respectively, when calculated with the four-parameter model.

Modified UNIFAC models

The UNIFAC model [25] is closely related to the UNIQUAC. The combinatorial term is the same as in eq. 15, but in the residual term the sum over components is replaced by the sum over groups in the molecules. Gabas and co-workers [26,27] used UNIFAC equations to describe the solubility of water + sucrose + glucose, water + sucrose + fructose, and water + xylose + mannose mixtures. Other authors prefer the modified UNIFAC model, proposed by Larsen et al. [21], because of its robustness with regard to temperature dependence [28].

In the modified UNIFAC model, the residual contribution to G_m^E is

$$\frac{G_m^{E\text{res}}}{RT} = \sum_k v_{k,i}\left(\ln\Gamma_k - \ln\Gamma_{k,i}\right) \tag{20}$$

where the summation extends over all groups k, Γ_k is the activity coefficient of group k at mixture composition, and $\Gamma_{k,i}$ is the activity coefficient of group k at a mixture composition corresponding to pure component i, and they are given by

$$\ln\Gamma_k = Q_k\left[1 - \ln\left(\sum_m \theta_m \psi_{km}\right) - \sum_m \frac{\theta_m \psi_{km}}{\sum_p \theta_p \psi_{pm}}\right] \tag{21}$$

where Q_k has the same meaning as in eq. 18, θ_m is the group analogous to the surface area fraction of eq. 17, except that it is defined in terms of the mole fraction of groups present in the solution [21], and ψ_{km} is similar to the Boltzmann factor, τ_{ij}, of eq. 19, except that it represents the interactions between groups k and m, and its temperature dependence is given by the same three parameters equation.

The classical groups of the modified model were CH_2, OH, and H_2O, while Catté et al. [29] introduced three new groups: the osidic bond (–O–), and the pyranose and furanose rings. This physicochemical UNIFAC model takes into account the conformational and solvation equilibria of the carbohydrate solutions.

The hydration numbers were set as the number of OH groups, which are not in an axial position for monosaccharides, and as the sum of the hydration numbers of the constituent monosaccharides less the number of equatorial OH groups used in the osidic bond for disaccharides. The interaction parameters a_{ij} are those of the original model [21] plus the water–group interactions, as summarized in Table 2. Note that $a_{ij3} = 0$ for the three new groups [29].

© 2010, IUPAC

Table 2 UNIFAC parameters for water + sugar mixtures from ref. [29]. The last two rows give the values of R_k and Q_k for each group.

		CH_2	OH	H_2O	PYR	FUR	–O–
CH_2	a_{ij1}/K		972.8	1857.0			
	a_{ij2}		0.2687	–3.322			
	a_{ij3}		8.773	–9.000			
OH	a_{ij1}/K	637.5		155.6			
	a_{ij2}	–5.832		0.3761			
	a_{ij3}	–0.8703		–9.0			
H_2O	a_{ij1}/K	410.7	–47.15		34.973	–183.901	–183.6655
	a_{ij2}	2.868	–0.4947		–0.22189	22.81	–2.5727
	a_{ij3}	9.0	8.65		0	0	0
PYR	a_{ij1}/K			–100.936			
	a_{ij2}			–0.221 89			
	a_{ij3}			0			
FUR	a_{ij1}/K			–183.901			
	a_{ij2}			–11.5571			
	a_{ij3}			0			
–O–	a_{ij1}/K			–183.6655			
	a_{ij2}			–2.5727			
	a_{ij3}			0			
R_k		0.6744	1.0	0.92	2.4784	1.8041	0.2439
Q_k		0.540	1.2	1.40	1.5620	1.106	0.442

Peres and Macedo [30] used the modified UNIFAC model for predicting solubility in binary and ternary mixtures of water with alcohols (methanol or ethanol) and/or carbohydrates (D-glucose, D-fructose, D-mannose, D-xylose, and sucrose). They proposed new temperature-independent interaction parameters, shown in Table 3, and introduced a new group, OH_{ring}, to account for proximity effects different from those of the usual alcohol group.

Table 3 UNIFAC parameters a_{ij} (in K) for water + sugar + alcohol mixtures from ref. [30].

	PYR	FUR	–O–	CH_2	OH	H_2O	OH_{ring}	CH_3	CH_3OH
PYR		0	0	0	0	–43.2789	0	0	0
FUR	0		0	0	0	–169.2309	0	0	0
–O–	0	0		0	–710.4904	0	0	0	–548.9565
CH_2	0	0	0		0	0	0	0	0
OH	0	0	–1700.0	0		0	596.4020	0	0
H_2O	–599.0453	–866.9163	0	0	0		–102.5464	0	0
OH_{ring}	0	0	0	0	213.8283	591.9366		0	564.6318
CH_3	0	0	0	0	0	0	0		0
CH_3OH	0	0	–687.9754	0	0	0	–76.9297	0	

In order to extend the UNIFAC model to the prediction of activity coefficients of fundamental biochemicals, Kuramochi et al. [31], introduced several new groups, including those for the enantiomeric discrimination of sugars, secondary amine, urea, guanidine, and inorganic ion groups. In the

case of ionic solutes like amino acid salts, an electrostatic contribution was added to the UNIFAC equation to account for the long-range electrostatic interactions.

A different group description, called S-UNIFAC, was used by Spiliotis and Tassios [32] for the description of mono- and disaccharides in alcohols and their mixtures with water. The new groups are CH_2OH, $CHOH_{axial}$, and $CHOH_{equatorial}$, which provide better predictions in non-aqueous solvents.

In the A-UNIFAC model [33], an association term, which only applies to the OH groups, is included. The model was applied to mixtures of sugars in mixed solvents (water and alcohols). More recently, Gros and co-workers [34] proposed an UNIFAC model that includes hydration equilibrium characterized by the hydration number and the hydration equilibrium constant. This hydration refers to the solute in solution, that is, different from the hydration of the solid solute defined above. This model was used to predict freezing point and solubility of binary aqueous solutions containing glucose, xylose, mannose, fructose, sucrose, maltose, lactose, and trehalose.

We will compare the predictions of the models described here with experimental results in Section 4.

Pitzer model

Another approach is based on the statistical theory of McMillan and Mayer [35], which considers the effective interactions between solute molecules averaged on all the solvent configurations, and yields the following expression for the excess Gibbs energy G^E per kg of solvent in the molal scale of solute concentration

$$\frac{G^E}{w_1 RT} = \sum_i \sum_j \lambda_{ij} m_i m_j + \sum_i \sum_j \sum_k \mu_{ijk} m_i m_j m_k + \ldots \tag{22}$$

where λ_{ij} represents the binary interaction between solute molecules, μ_{ijk} arises from triple interactions, etc. Strictly, the McMillan Mayer theory of solutions is cast in a reference framework where the concentration of the solute should be expressed in molarity and the chemical potential of the solvent is kept constant. Thus, the excess Gibbs energy is calculated for a pressure equal to the sum of the solvent vapor pressure plus the osmotic pressure of the solution, in contrast to the conventional Lewis–Randall reference system where the properties are calculated in molality at constant pressure. The conversion factors between both reference systems could be quite different from unity in concentrated solutions, but usually the correction is ignored and could be absorbed in the empirically adjusted virial coefficients (λ, μ,…), which are concentration-dependent.

The osmotic coefficient of the solution, related to the solvent activity, and the activity coefficients (molal scale) of the solutes can be obtained [10] by differentiation of G^E

$$\phi = -\left(\frac{1}{M_1 \sum_{i>1} m_i}\right) \ln a_1 = 1 - \frac{\left(\partial G^E / \partial w_1\right)_{n_i}}{RT \sum_{1>1} m_i} \tag{23}$$

$$\ln \gamma_i = \left[\frac{\partial\left(G^E / w_1 RT\right)}{\partial M_i}\right]_{w_1, n_{j\neq i}} \tag{24}$$

which consistently obey the Gibbs–Duhem relationship. For an aqueous solutions containing just one solute, this relationship establishes that we can obtain the solute activity coefficient if the osmotic coefficient is known and vice versa.

In practice, the carbohydrate solutions frequently contain ionic solutes, which modify the excess Gibbs energy of the mixture and, consequently, the osmotic and activity coefficients. Pitzer [36] ex-

tended eq. 22 for the case of mixtures of electrolytes and non-electrolytes by adding terms for cations (c) and anions (a) and their interactions with neutral solutes (n)

$$\frac{G^{\mathrm{E}}}{w_1 RT} = f(I) + 2\sum_{\mathrm{c}}\sum_{\mathrm{a}} m_{\mathrm{c}} m_{\mathrm{a}} \left[B_{\mathrm{ca}} + \left(\sum_{\mathrm{c}} m_{\mathrm{c}} z_{\mathrm{c}} \right) C_{\mathrm{ca}} \right] + \sum_{\mathrm{c}} \sum_{\mathrm{c}'<\mathrm{c}} m_{\mathrm{c}} m_{\mathrm{c}'} \left[2\Phi_{\mathrm{cc}'} + \sum_{\mathrm{a}} m_{\mathrm{a}} \Psi_{\mathrm{cca}'} \right] +$$
$$\sum_{\mathrm{a}} \sum_{\mathrm{a}'<\mathrm{a}} m_{\mathrm{a}} m_{\mathrm{a}'} \left[2\Phi_{\mathrm{aa}} + \sum_{\mathrm{c}} m_{\mathrm{c}} \Psi'_{\mathrm{caa}'} \right] + 2\sum_{\mathrm{n}}\sum_{\mathrm{c}} m_{\mathrm{n}} m_{\mathrm{c}} \lambda_{\mathrm{nc}} + 2\sum_{\mathrm{n}}\sum_{\mathrm{a}} m_{\mathrm{n}} m_{\mathrm{a}} \lambda_{\mathrm{na}} + \tag{25}$$
$$2\sum_{\mathrm{n}} m_{\mathrm{n}}^2 \lambda_{\mathrm{nn}} + 2\sum_{\mathrm{n}}\sum_{\mathrm{n}'} m_{\mathrm{n}} m_{\mathrm{n}'} \lambda_{\mathrm{nn}'} + \ldots$$

where the terms involving triple interactions, not shown here, are usually negligible. The function $f(I)$ includes the Debye–Hückel limiting law, and it depends only on the ionic strength and not on individual molality or other solute properties

$$f(I) = -\left(\frac{4IA_\phi}{b} \right) \ln\left(1 + bI^{1/2} \right) \tag{26}$$

with A_ϕ being the Debye–Hückel limiting slope, b = 1.2 kg$^{1/2}$ mol$^{-1/2}$ and I = ½Σ$m_i z_i^2$, with z_i the ion charge.

The ion–ion interaction coefficients, B_{ca}, are also a function of the ionic strength

$$B_{\mathrm{ca}} = \beta^{(0)} + \beta^{(1)} g\left(\alpha_1 I^{1/2} \right) + \beta^{(2)} g\left(\alpha_2 I^{1/2} \right) \tag{27}$$

with

$$g(x) = \frac{2}{x^2}\left[1 - (1+x)\exp(-x) \right] \tag{28}$$

where α_1 and α_2 are constants. Usually, the term $\beta^{(2)}$ in eq. 27 is unnecessary for fully dissociated electrolytes, being α_1 = 2.0 kg$^{1/2}$ mol$^{-1/2}$. Moreover, the binary and ternary interaction coefficients for the ionic species are given by

$$\phi_{\mathrm{cc}'} = \lambda_{\mathrm{cc}'} - \left(\frac{z_{\mathrm{c}'}}{2z_{\mathrm{c}}} \right) \lambda_{\mathrm{cc}} - \left(\frac{z_{\mathrm{c}}}{2z_{\mathrm{c}'}} \right) \lambda_{\mathrm{c}'\mathrm{c}'} \tag{29}$$

$$\Psi_{\mathrm{cc}'\mathrm{a}} = 6\mu_{\mathrm{cc}'\mathrm{a}} - \left(\frac{3z_{\mathrm{c}'}}{z_{\mathrm{c}}} \right) \mu_{\mathrm{cca}} - \left(\frac{3z_{\mathrm{c}}}{z_{\mathrm{c}'}} \right) \mu_{\mathrm{c}'\mathrm{c}'\mathrm{a}} \tag{30}$$

Pitzer's ion-interaction approach for describing mixtures of carbohydrates and electrolytes could be an interesting alternative to other empirical virial expansions. We will discuss this point at the end of this section, after reviewing such empirical approaches.

Empirical virial expansions

Robinson et al. [37] and Herrington and Meunier [38] studied the osmotic coefficient of aqueous mixtures of sucrose with NaCl and KCl, and they defined an experimental quantity as

$$\Delta_{\mathrm{en}} = \frac{1}{m_{\mathrm{e}} m_{\mathrm{n}}} \left(\nu_{\mathrm{r}} m_{\mathrm{r}} \phi_{\mathrm{r}} - m_{\mathrm{n}} \phi_{\mathrm{n}}^o - \nu m_{\mathrm{e}} \phi_{\mathrm{e}}^o \right) = \sum_{p,q} X_{p,q} m_{\mathrm{n}}^p m_{\mathrm{e}}^q \tag{31}$$

where the subscript r refers to the reference solution used in the isopiestic experiments and $\phi^{o}{}_i$ is the osmotic coefficient of the aqueous binary solution of pure component i. Thus, Δ_{en} represents the excess

osmotic coefficient, which is empirically expressed as a power series in the molality of the electrolyte (m_e) and the non-electrolyte (m_n) components, $X_{p,q}$ being coefficients. By applying the Gibbs–Duhem equation, the excess Gibbs energy of the components can be expressed as

$$\frac{\mu_n^E}{RT} = \frac{\mu_n^{*E}(m_n)}{RT} + \sum_{p,q} \frac{p+1}{p+q+1} X_{p,q} m_n^p m_e^{q+1} \tag{32}$$

$$\frac{\mu_e^E}{RT} = \frac{\mu_e^{*E}(m_e)}{RT} + \frac{1}{v} \sum_{p,q} \frac{q+1}{p+q+1} X_{p,q} m_n^{p+1} m_e^q \tag{33}$$

where μ_i^{*E} represents the excess chemical potential of the component i in the binary aqueous solution.

Alternatively, the interactions between non-electrolytes and electrolytes can be expressed in terms of the standard Gibbs energy for transferring the electrolyte and the non-electrolyte from pure water to the electrolyte/non-electrolyte/water mixture [39–41]

$$\Delta_t G_e = \mu_e(m_n, m_e) - \mu_e^*(m_e) = 2v g_{en} m_n + 3v g_{enn} m_n^2 + 3v^2 g_{een} m_n m_e + \ldots \tag{34}$$

$$\Delta_t G_n = \mu_n(m_n, m_e) - \mu_n^*(m_n) = 2v g_{en} m_e + 3v^2 g_{een} m_e^2 + 3v g_{enn} m_n m_e + \ldots \tag{35}$$

v being the number of ions into which the electrolyte dissociates and g_{en}, g_{enn}, and g_{een} are the binary and ternary interaction coefficients, respectively. These interaction coefficients can be expressed in terms of the interactions between the corresponding cation and anion with the sugar. Thus, for instance: $vg_{es} = \nu_c g_{cs} + \nu_a g_{as}$, where ν_c and ν_a are the stoichoimetric numbers of cation and anion in the electrolyte, respectively.

For standard functions, the higher terms in m_e and m_n on the right side of eqs. 34 and 35 vanish, and the limiting slopes of the standard transfer coefficients, g_{en}, must be identical for both functions.

Morel and co-workers [42–49], Wang and co-workers [50–61], and Hernandez-Luis et al. [62,63] used the transfer functions approach and reported a very comprehensive set of data for the interaction parameters of sugars with several electrolytes.

On the other hand, the use of the Pitzer approach for ternary water + sugar + electrolyte solutions in the form given by eq. 25 has not been analyzed in the literature. Actually, a few works deal with Pitzer equations in aqueous sugar + electrolytes mixtures, and all of them treat the system as a pseudo-binary system, that is, the mixture water + sugar is considered as a pure solvent with the dielectric and viscosity properties of the mixture. Thus, the experimental activity coefficients of NaCl in glucose, sucrose, and fructose aqueous solutions [52,63] and $CaCl_2$ in maltose and lactose aqueous solutions [61] at 25 °C were described using Pitzer pseudo-binary coefficients with an accuracy similar to the transfer functions approach given by eqs. 34–35.

3. THEORETICAL MODELS FOR PREDICTING NON-EQUILIBRIUM-PHASE TRANSITIONS IN AQUEOUS SYSTEMS

In this section, we describe different available models for predicting the glass transition and maximally freeze-concentrated points. In this way, we complete the basic information to obtain SPDs in aqueous systems.

3.1 Glass transition models

The glass transition temperature of a binary mixture is usually estimated by resorting to two different theoretical approaches: (i) models based on the free volume theory of liquids [64]; (ii) models that treat

the glass transition as an Ehrenfest second-order transition in which the enthalpy, entropy, and volume of the mixture are continuous at T_g [65].

Models of the first group, like the Gordon and Taylor model (GTM), have been originally developed to predict the glass transition temperature of polymer blends [66]. The T_g of the mixture can be calculated from the T_g values of the pure components through the equation

$$T_g = \frac{w_2 T_{g2} + w_1 k_{GT} T_{g1}}{w_2 + w_1 k_{GT}} \tag{36}$$

where w_1 and w_2 are the mass fractions of water and solute, respectively. The adjustable parameter k_{GT}, which expresses the degree of curvature of the T_g-composition dependence, can be semi-quantitatively related to the strength of the interaction between the two components [66]. It can be seen that when $k_{GT} = 1$, a simple mixing rule (linear model) is obtained. However, when the degree of interaction is composition-dependent, positive or negative deviations from the simple mixing rule are observed, and usually $k_{GT} \neq 1$.

The coefficient k_{GT} can be calculated from the densities of the components and the change of the thermal expansibility, $\Delta\alpha$, at T_g. Using the Simha–Boyer rule [67] that establishes that $\Delta\alpha T_g \approx$ constant, it results

$$k_{GT} = \frac{\rho_2 T_{g2}}{\rho_1 T_{g1}} \tag{37}$$

An empirical equation proposed by Jenckel and Heusch [68] expressed in terms of the weight fractions

$$T_g = w_1 T_{g1} + w_2 T_{g2} + k w_1 w_2 \tag{38}$$

has also been successfully used for different binary mixtures, but it fails when applied to low-molar-mass liquids [69] as also observed with eq. 36.

The Couchman–Karasz model (CKM) treats the glass transition as an Ehrenfest second-order transition [70,71]. The CKM expression for T_g of the mixture as a function of composition is given in terms of the glass transition temperatures of the pure solution components and their corresponding heat capacity change at the glass transition, $\Delta C_{p,i} = C_{p,i}(\text{liq}) - C_{p,i}(\text{glass})$, assumed independent of the temperature.

$$\ln T_g = \frac{w_1 \Delta C_{p,m,1} \ln T_{g1} + w_2 \Delta C_{p,m,2} \ln T_{g2}}{w_1 \Delta C_{p,m,1} + w_2 \Delta C_{p,m,2}} \tag{39}$$

This equation is identical to that derived by Gordon et al. [72] from the Gibbs–DiMarzio theory of the glass transition and to the empirical equations quoted by these authors.

A modification of the CKM due to Ten Brinkle, Karasz, and Ellis [73] assumes that the heat capacity changes are proportional to the temperature. The modified CKM gives the following expression for T_g:

$$T_g = \frac{w_2 T_{g2} + w_1 k_{CK} T_{g1}}{w_2 + w_1 k_{CK}} \tag{40}$$

where

$$k_{CK} = \frac{\Delta C_{p,m,1}}{\Delta C_{p,m,2}} \tag{41}$$

Note that eqs. 36 and 40 are similar, except that k_{GT} and k_{CK} can be predicted from volumetric and thermal experimental properties of the pure components, respectively.

An extension of the GTM was proposed by Kwei [74], also for polymer mixtures, which contains a term accounting for the interaction between water and solute

$$T_g = \frac{w_2 T_{g2} + w_1 k T_{g1}}{w_2 + w_1 k} + q w_1 w_2 \tag{42}$$

where q is an adjustable parameter, positive or negative, depending on the solute–solute interactions. For mixtures of water and polyols, it is expected that the strong hydrogen bonds lead to large positive values for this parameter. It should be noted that Kwei's equation for $k = 1$ reduces to the Jenckel and Heusch, eq. 38.

Matveev et al. [75] developed an additive group-contribution model (AGCM) to predict the glass transition temperature of mixtures of biopolymers, including polysaccharides, and water. The model has parameters, which can be obtained from the structure of the polysaccharide, such as ν_o, the ratio between the molar mass of the monomeric unit and water, or $\langle n \rangle$, the mean number of hydrogen bonds into monomeric units. Other parameters are related to the effect of water on the hydrogen bonds and dipole–dipole interactions between monomeric units in the polysaccharide, given by the functions f_h and f_e, respectively.

The final expression is given in the form of the plasticization function

$$\frac{T_g}{T_{g2}} = \frac{f_h}{1 + \left(1 - f_e\right) f_h T_{g2} \left\langle T_{gd}^{-1} \right\rangle} \tag{43}$$

with

$$f_h = \left[1 + \left(\frac{w_1}{1 - w_1} \right) \nu_o K_h T_{g2} \left\langle T_{gh}^{-1} \right\rangle \right]^{-1} \tag{44}$$

$$f_e = 1 + \frac{3\beta}{1 - \beta + 3/\left(\varepsilon_2 / \varepsilon_1 - 1\right)} \tag{45}$$

where $K_h = 4$ is the number of hydrogen bonds blocked by a water molecule, ε_1 and ε_2 are the permittivity of the water and polysaccharide, respectively. The $\langle {T_{gd}}^{-1} \rangle$ and $\langle {T_{gh}}^{-1} \rangle$ are adjustable parameters related to the dipole–dipole and hydrogen bond effect of water on the solute, and

$$\beta = \frac{w_1 \left(V_1 / V_2\right)}{w_1 \left(V_1 / V_2\right) + w_2 v_0} \tag{46}$$

V_1 and V_2 being the van der Waals volume of water and monomeric unit, respectively.

3.2 Prediction of the maximally freeze-concentrated point

The studies by Levine and Slade [1–5] showed that the maximally freeze-concentrated point, T_g', is the most noteworthy feature of low-temperature DSC thermograms, corresponding to the intersection of an extension of thermodynamically defined equilibrium ice-melting curve and the kinetically determined supersaturated glass transition curve, and it is a quasi-invariant point in the state diagram for any particular solute. The C_g' is independent of the initial solute concentration, while the amount of ice formed does depend on the initial concentration.

© 2010, IUPAC

Levine and Slade reported T_g' values for 24 small carbohydrates and other low-molar-mass polyhydroxy compounds [4]. The T_g' values for maximally frozen 20 wt % solutions exhibit a reasonable linear correlation with the inverse of the solute molar mass ($r = 0.95$), but this linear correlation is even better ($r = 0.99$), when the single homologous family of glucose and its linear malto-oligomers up to maltoheptaose is considered. Other correlations have been proposed taking into account W_g', the grams of unfrozen water (UFW) per gram of solute [5] which allows the calculations of weight-averaged or number-averaged molar masses of solute and UFW. Satisfactory correlations ($r = 0.95$) were obtained when T_g' was plotted as a function of the inverse of the weight-averaged molar mass.

Another approach proposed by Matveev and Ablett [76] uses a water-clustering theory [77], developed by Matveev, to describe the change of the glass transition temperature of the unfrozen water with the cluster size. The model requires the parameters $z = T_{g2}/T_{g1}$ and $K_2 = \Delta C_{p,m,2}/\Delta C_{p,m,1}$, which are related to each other by

$$6.986K_2(z-1)z = (zK_2 - 1)zf(y) + 1.819f(y)(2.645 - y)^{-0.5} \tag{47}$$

where $f(y) = \ln\{2y^{1.5}[(1.55y^{0.5} - 1)^3 + 1/3]\}$, $y = N/N_c$ being the ratio between the number of molecules, N, in the cluster of water in the solution and the critical number of molecules of water, N_c, that is, T_g becomes independent of N for $N > N_c$. Once y is calculated from the values of z and K_2, the maximally freeze-concentrated point can be evaluated from the following expressions

$$\frac{T_{g1}}{T_g'} = 1 - 0.145f(y) \tag{48}$$

$$C_g' = 0.55z(2.645 - y)^{0.5} \tag{49}$$

Matveev [77] showed that K_2 can be expressed in terms of z and a parameter, k, depending on the chemical structure of the solute

$$K_2 = \frac{w_1}{z(1-w_1)}\left[\frac{z-1}{zB} - 1\right] \tag{50}$$

where $B = (0.0868z - 0.0619)/[1 + 0.063(z - 1/k)]$, and $k = 0.366$ for saccharides.

Finally, the prediction of the non-equilibrium freezing curve described in Section 2.1 can be extended from the eutectic point to the intersection with the glass transition temperature in order to obtain the maximally freeze-concentrated point. This approach will be suitable provided that T_g' is not lower than –50 °C, the limit of validity of eq. 6.

It should be noted, according to the discussion on the difference between T_g' and T_m' in Section 1 (see Fig. 1), that this procedure could lead to an underestimation of T_g' (overestimation of C_g'), particularly in the case of low-molar-mass saccharides.

4. RESULTS

Many types of solutes are used in aqueous solutions as cryoprotectants of food and biological materials, including mono- and disaccharides (glucose, fructose, sucrose, trehalose), olygosaccharides (raffinose), polyols (glycerol, sorbitol, mannitol, propylene glycol), dimethyl sulfoxide (DMSO), and poly(vinylpyrrolidone) (PVP).

In this section, we will compare the prediction of the models discussed above for the equilibrium and non-equilibrium curves of the state diagram of freezing in aqueous solutions with the experimental results, taking the carbohydrates as representative cryoprotectants, because they are widely used in practical cases and there are abundant experimental information on the properties of these mixtures.

4.1 Freezing point and carbohydrate solubility in aqueous solutions

Most of the theoretical predictions of freezing point and solubility of carbohydrate aqueous solutions have been applied to glucose, fructose, and sucrose. Thus, the pioneering work by Chandrasekaran and King [78] used eq. 4 and the regular model of multicomponent solutions for the activity coefficients of water and saccharides to predict solid + liquid equilibrium in solutions of fruit juices containing different proportions of the sugars listed above. We will include trehalose in this group because it is a sugar that seems to have enhanced cryoprotectant properties in comparison with other sugars.

The source of experimental data for carbohydrate + water mixtures is very comprehensive. Goldberg and Tewari [79] reviewed thermodynamic properties of the five- and six-membered ring carbohydrates in both condensed and aqueous phases, including D-glucose and D-fructose. The α-D-glucose exists as both a monohydrate and in the anhydrous form, while β-D-glucose only has the anhydrous form. D-fructose exhibits a more complex phase behavior with the presence of gel, anhydrous, metastable crystalline, hemihydrate, and dihydrate phases.

The ice-melting curve and the solubility curve of the glucoses and fructoses were reported by Young and co-workers [80,81].

The equilibrium-phase diagram of sucrose was reported by several authors [82–87], including the solubility of the anhydrous, and the different hydrated forms. Ice-melting curves of sucrose + NaCl + water mixtures were reported by Gayle et al. [88] all over the range of mole ratios of NaCl/sucrose in aqueous NaCl + sucrose solutions, and also by Shalaev and Franks [89], who reported several binary and ternary eutetic and peritectic points, taking into account the existence of NaCl, sucrose, and NaCl + sucrose hydrates.

There is abundant information on the ice-melting curve and the solubility curves of anhydrous and dihydrate α,α-trehalose, attesting to its popularity as a cryoprotectant and stabilizer during dehydration and anhydrobiosis. Chen et al. [90] reviewed all the reported data and found a good agreement among these for the ice-melting curve [91–93], although the data reported by Nicolajsen and Hvidt [91] showed lower ice-melting temperatures, particularly at higher trehalose concentration than other studies. Also, the solubility values reported by Nicolajsen and Hvidt [91] are much higher than those from other authors [92–94] and have been discarded in the comparison. Moreover, the solubility data by Lammert et al. [94] seem to deviate from the previous studies [92,93], which extend over a wider range of trehalose composition. The isomer β,β-trehalose, which forms a tetrahydrate, was also studied [95] but the information is limited because this sugar does not occur naturally but must be chemically synthesized.

Catté et al. have calculated the freezing curves of sucrose, glucose, and fructose aqueous mixtures using UNIQUAC [17], and sucrose and glucose aqueous mixtures using UNIFAC [29], with the interaction parameters reported in Tables 1 and 2. The calculation extends up to sugar concentration below the eutectic point for glucose and sucrose, but goes beyond the eutectic point for fructose. The results are in excellent agreement with the experimental values, except for fructose solutions with $w_2 > 0.5$, that is, well above the eutectic concentration, where the model slightly overestimates the freezing depression.

The results reported by Ben Gaida et al. [34] for sucrose and glucose concentrations below the eutectic point, using the UNIFAC model including hydration, also show a good agreement with the experimental data.

Blond et al. [96] extended the calculation of the freezing curve for sucrose aqueous mixtures above the eutectic point (up to $w_2 = 0.79$) using UNIQUAC with the interactions parameters reported in Table 1 [17]. The results, shown in Fig. 2, indicate that above $w_2 = 0.7$, the predicted fusion temperature decreases are slightly larger than experimentally observed. The modification of the UNIQUAC parameters, including extra experimental data [96], worsens the deviation in the concentrated region.

Perez and Macedo calculated the freezing curves of sucrose, glucose. and fructose aqueous mixtures using UNIQUAC [23] and UNIFAC [30]. They found an excellent agreement with the experimental results for glucose and fructose up to $w_2 = 0.7$, that is, well beyond the eutectic points. However,

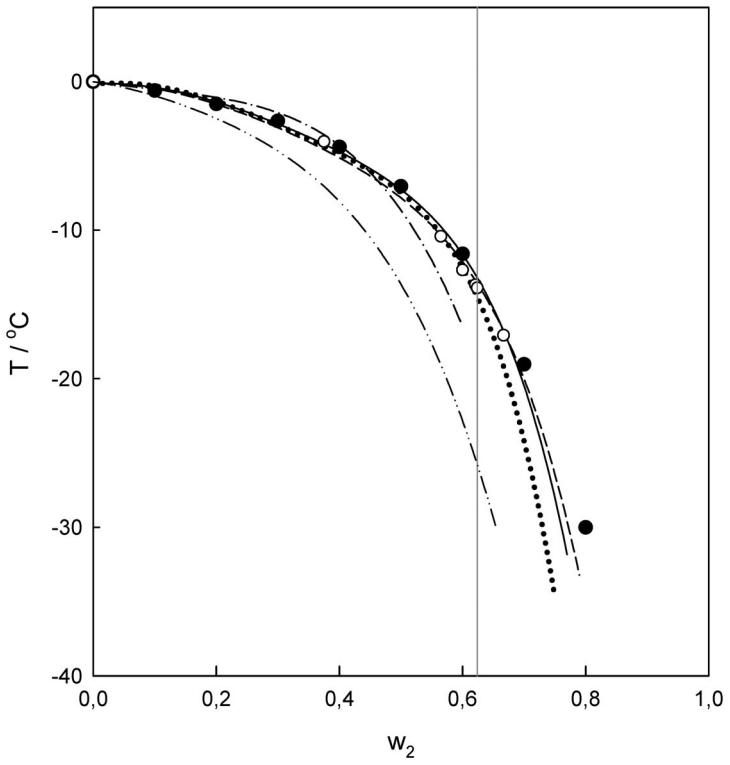

Fig. 2 Temperature vs. mass fraction of sucrose to illustrate the ice-melting curve for sucrose aqueous solutions. Experimental data: (●) [82]; (○) [87] (the vertical gray line indicates the eutectic point). Predicted by: UNIQUAC [96] (dashed line); UNIQUAC [23] (solid line); UNIFAC [30] (dotted line); S-UNIFAC [32] (dashed–dotted line); TIEC [97] (dashed–dotted–dotted line).

the results for sucrose using both models overestimate the freezing depression above $w_2 = 0.7$, as found by Blond et al. [96], the predictions of the UNIFAC model being worse than those of the UNIQUAC (see Fig. 2) due to the fact that the latter one has temperature-dependent interaction parameters.

The S-UNIFAC model [32] predicts the freezing point of glucose and fructose up to the eutectic concentration, but slightly overestimates it at higher concentrations. For sucrose, as shown in Fig. 2, the overestimation occurs at $w_2 > 0.4$, that is, below the eutectic point.

The predictions of the TIEC model [16,97], which has no adjustable parameters, are also shown in Fig. 2. It can be seen that this model largely overestimates the freezing depression in sucrose aqueous solutions, as well in glucose aqueous solutions.

The capability of the above-mentioned models to predict the solubility of saccharides in aqueous solutions will be analyzed, although this solid + liquid equilibrium is not so relevant in cryopreservation as it is for the ice-melting/freezing curve, particularly in the metastable region, at solute concentrations beyond the eutectic point.

Figure 3 shows the solubility and ice-freezing curves of glucose (monohydrate and anhydrous) and fructose (dihydrate and anhydrous) calculated using the theoretical models, compared to the experimental values. The ice-freezing curves for both monosaccharides, which extend beyond the eutectic points, are well described using the UNIQUAC models [17,23], and also the UNIFAC model [30], not shown in Fig. 3.

© 2010, IUPAC

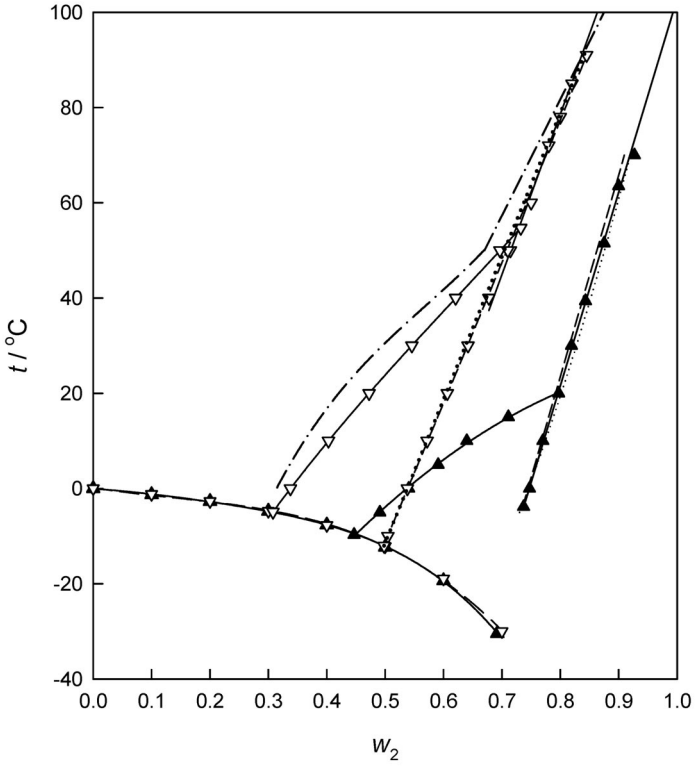

Fig. 3 Fusion and solubility temperatures vs. mass fraction of sugar to illustrate sugar solubility and ice-freezing curves for fructose and glucose. Experimental data: (▲) dihydrate and anhydrous fructose [27,81]; (▽) monohydrate and anhydrous glucose [80]. Predicted by: UNIQUAC [17] (solid line); UNIQUAC [23] (dashed line); UNIFAC [30] (dotted line); TIEC [97] (dashed–dotted line).

The solubility curves calculated with UNIQUAC and UNIFAC models agree within the experimental error with the experimental data. On the other hand, the TIEC model applied to the solubility of monohydrate and anhydrous glucose underestimates the solubility over all the range of temperatures.

4.2 Glass transition temperature

In this section, we will compare the predictions of the glass transition temperatures of aqueous solutions of saccharides using the theoretical models discussed in Section 3.1. In all of these models, information is required on the properties of water and the solute at the glass transition temperature. Thus, the GTM (eqs. 36 and 37) is based on the volumetric properties, the CKM (eqs. 39–41) on the calorimetric changes, and the AGCM (eqs. 43–46) on the dielectric and hydration properties.

Glass transition of pure water

The averaged glass transition temperature of pure water reported for amorphous solid water [98–101] and for hyperquenched water [101–106], T_{g1} = 136 K, has been adopted, but it is important to keep in mind that the properties of this glass transition are not those to which one is accustomed, when dealing with aqueous solutions. For this reason, the value of the heat capacity change at T_g that is adopted for our solutions calculations is not the value that is measured at the experimental glass transition for water, which we now discuss.

The value of $\Delta C_{p,m,1}$ for pure water has been studied by many authors with very different results. For instance, in the study of Sugisaki et al. [98], in which the water was vapor-deposited into the adia-

batic calorimeter sample compartment, it was large, $\Delta C_{p,m,l}$ = 35 J K^{-1} mol^{-1} while in the study of MacFarlane and Angell [99], in which the vapor deposition was made directly into a DSC sample pan, no C_p increase at all could be detected down to the instrument sensitivity limit of 0.36 J K^{-1} mol^{-1}. Subsequent measurements by Hallbrucker et al. [100], using special annealing techniques to enhance the relaxation strength, subsequently yielded a value of 1.6 J K^{-1} mol^{-1} for hyperquenched glassy water.

The most recent value, obtained without annealing on a sample vapor deposited at 140 K, is even smaller, 0.70 J K^{-1} mol^{-1} at a T_g value of 140 K [107]. This is to be compared with the values (20 ± 0.9) J K^{-1} mol^{-1} expected by extrapolation to pure water, of measurements made over a range of compositions of several glass-forming aqueous salt systems [108]. Even larger values, 35 J K^{-1} mol^{-1}, are indicated by the observations on binary molecular solutions such as those of the $H_2O + H_2O_2$ and $H_2O + N_2H_4$ systems [109]. The physical reason for these discrepancies is unfortunately hidden in the inaccessible regime imposed by the 10^5 K s^{-1} hyperquenching needed for vitrification (or crystallization of ice in the case of reheating or dilution). A "fragile-to-strong" liquid transition in the "no-man's land" with dramatic C_p decrease seems the most likely explanation [110,111], though a hidden glass transition of larger magnitude within the "no-man's land" has also been suggested on the basis of hyperquenched inorganic glass studies [112].

Since it is the fragile liquid heat capacity that is relevant to solution studies, it is the latter value, 35 J K^{-1} mol^{-1}, that is most appropriate for calculations using the CKM equation for molecular solutions, though a smaller value would be recommended for solutions in which salts are a component.

The GTM requires information on the volumetric properties of water and the solute at the glass transition temperature, which is not always available. Thus, the density of amorphous ice differs according to the preparation method, and can vary from 0.94 g cm^{-3} for low-density amorphous (LDA) ice to 1.17 g cm^{-3} for high-density amorphous (HDA) ice [113], while the density of supercooled water decreases from 1.00 to 0.977 g cm^{-3} as temperature decreases from 0 to –35 °C [114,115].

Glass transition predictions of saccharide aqueous solutions

The application of the GTM is limited due to the lack of information on the density of the saccharides in the supercooled regime. Only in the case of trehalose aqueous solutions, the partial molar volume of the sugar is known at temperatures down to –15 °C [92], which allows reliable extrapolations to the glass transition temperatures of its aqueous solutions. Even in this case, the uncertainty of the prediction using eq. 37 to obtain the parameter k_{GT} is very large.

Roos [7] proposed that this parameter could be obtained empirically for saccharide aqueous solutions by fitting k_{GT} using the measured glass transition of these systems to eq. 36. A linear relationship was found between this parameter and the glass transition temperature of the sugar

$$k_{GT} = 0.0293 T_{g2} - 4.39 \tag{51}$$

Figures 4 and 5 show the experimental values of the glass transition temperatures reported for aqueous sucrose and trehalose solutions, respectively. Only data reported numerically in the literature were included in these figures, and all of them were obtained from DSC. In the case of sucrose, the difference between T_g obtained from midpoint [7,116–121] and onset* [85,86,122–125] is significant, while for trehalose the range of composition for the data obtained from midpoint [7,92,123,126] and onset [7,118,121,127–130] do not overlap and a common fit was possible all over the range of compositions. The T_{g2} values for both pure saccharides are (341 ± 7) K (onset) and (346 ± 6) K (midpoint) for sucrose, and (389 ± 3) K (onset and midpoint) for trehalose.

*Glass transition temperatures from a DSC (heating) scan are obtained from the temperature at which the slope of the heat flow starts changing (onset), the temperature where the heat flow change is half of the total (midpoint), or the temperature where the change ends (endpoint).

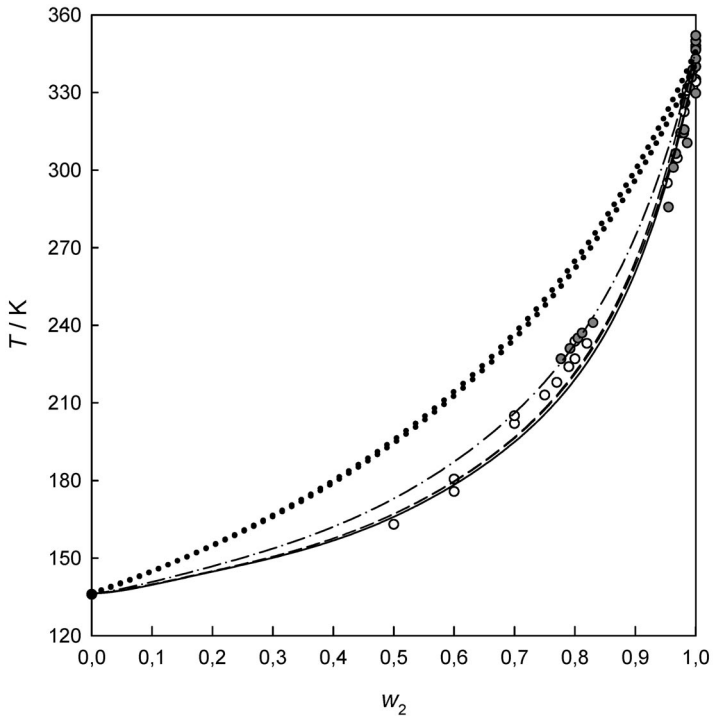

Fig. 4 Glass transition temperature vs. mass fraction of sucrose in sucrose + water solutions. Experimental data: (○) midpoint [7,116–121]; (●) onset [85,86,122–125]. Solid and dashed–dotted lines correspond to the best fit of midpoint (T_{g2} = 346 K; k_{GT} = 5.82) and onset (T_{g2} = 341 K; k_{GT} = 4.67) glass transition temperature, respectively; dashed line correspond to the fit using eq. 36 with k_{GT} given by eq. 51; dotted lines correspond to the fit using eq. 40 with the k_{CK} given by eq. 41 and T_{g2} = 341 K and T_{g2} = 346 K.

The predictions for sucrose solutions using the empirical k_{GT} given by eq. 51 are shown in Fig. 4 for T_{g2} = 341 K, although a similar result is obtained using the midpoint average value for pure sucrose. The agreement is good, but it should be considered with caution because sucrose was one of the saccharides included among the low-molar-mass carbohydrates used in the fit. In the case of trehalose solutions, the empirical k_{GT} obtained with T_{g2} = 380 K for pure trehalose reported by Roos [7] is underestimated when compared to the most recent glass transition measurements in the water-rich region.

The CKM T_g predictions, also shown in Figs. 4 and 5, were performed by using $\Delta C_{p,m,2}$ = 215 J K^{-1} mol^{-1} for trehalose [92] and $\Delta C_{p,m,2}$ = 264 J K^{-1} mol^{-1} for sucrose [131], while for water we adopted $\Delta C_{p,m,1}$ = 35 J K^{-1} mol^{-1}, that is the value reported for aqueous solutions. Therefore, k_{CK} in eq. 41 is 3.10 and 2.52 for trehalose and sucrose, respectively.

It is clear that the CKM predictions largely overestimate the glass transition temperature of both disaccharides all over the composition range, as already noted by Blond et al. [96] for sucrose aqueous solutions.

It could be argued that the choice of $\Delta C_{p,m,1}$ as that reported for aqueous solutions, instead of the much smaller values reported for annealed amorphous or hyperquenched glassy water, could be responsible for the disagreement. However, if the ΔC_{p1} measured for pure amorphous or hyperquenched water is used in eq. 41, $k_{CK} < 1$ is obtained, which results in convex curves instead of the concave curves experimentally observed.

© 2010, IUPAC

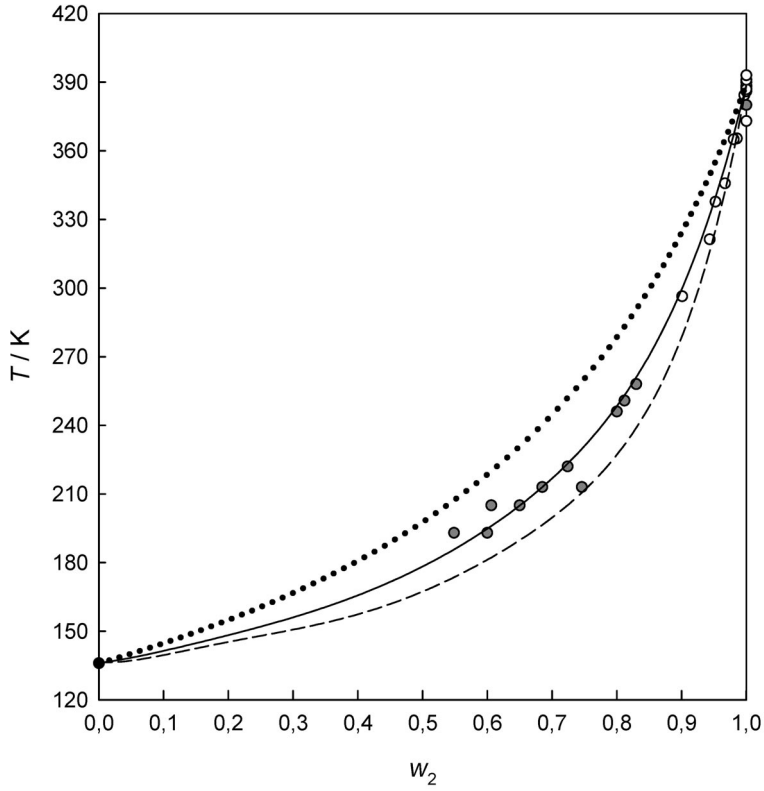

Fig. 5 Glass transition temperature of trehalose vs. mass fraction of trehalose in trehalose + water solutions. Experimental data: (○) midpoint [7,92,123,126]; (●) onset [7,118,121,127–130]. Solid line corresponds to the best fit of midpoint and onset (T_{g2} = 389 K; k_{GT} = 4.98) glass transition temperature; dashed line corresponds to the fit using eq. 36 with k_{GT} given by eq. 51; dotted lines correspond to the fit using eq. 40 with the k_{CK} given by eq. 41 (see text).

Katkov and Levine [132] have analyzed recently the GTM (eqs. 36 and 37) and the different formats of the CKM (eqs. 39–41) for predicting T_g, using water + trehalose as a test system. Unfortunately, the comparison of the theoretical models is restricted to this particular system that, as mentioned before, is one of the systems having a large scatter of T_g values. Moreover, no direct comparison with experimental data of T_g for trehalose aqueous solutions has been performed by these authors, but with the best fit reported by Chen et al. [90] using the GTM (k_{GT} = 6.54). The more important conclusion of the Katkov and Levine analysis, related to T_g prediction in the trehalose + water system, is that the original CKM expression (39) fits the experimental data using the available $\Delta C_{p,m,1}$ and $\Delta C_{p,m,2}$ data, while the modified CKM equation (40) overestimates the T_g of the mixtures.

In Table 4, the values of $\Delta C_{p,m,2}$ reported in the literature for sucrose [7,123,132] and trehalose [7,92,127,129,133] and the calculated values of k_{CK} are summarized. A large scatter in the changes of heat capacities, and consequently in k_{CK}, is observed for these sugars. Similar differences were observed for other saccharides and polyols [132].

© 2010, IUPAC

Table 4 Parameters of the CKM for sucrose and trehalose.

Compound	T_g/K	ΔC_p/J K^{-1} mol^{-1}	k_{CK}	Ref.
Water	136	35		100,108
Sucrose	335 (o)	195	3.40	133
	343 (m)	264	2.52	124
	335 (o)	205	3.23	7
Trehalose	373 (o)	188	3.55	133
	388 (m)	216	3.10	92
	373 (o)	188	3.55	7
	387 (o)	222	2.98	127
	386,388 (o)	202	3.29	129

(o) onset; (m) midpoint

The AGCM (eqs. 43–46) was tested by Matveev et al. [75] for polysaccharides such as amylose, amylopectin, dextran, and pullulan. The parameter $\langle T_{gh}{}^{-1} \rangle$ was fixed at 0.2028 10^{-3} K^{-1} for all the polysaccharides, while $\langle T_{gd}{}^{-1} \rangle$ ranges from 0.29 K^{-1} (dextran and pullulan) to 0.31 K^{-1} (amylose and amylopectin). The maximum difference between calculated and experimental glass transition temperatures is about (10–30) K, which is comparable to errors introduced through experimental accuracy.

A detailed comparison of the CKM and AGCM is possible using the experimental data by Bizot et al. [134] for amylose in the range w_2 = 0.80–0.95. Figure 6 shows the best CKM fit along with the AGCM predictions.

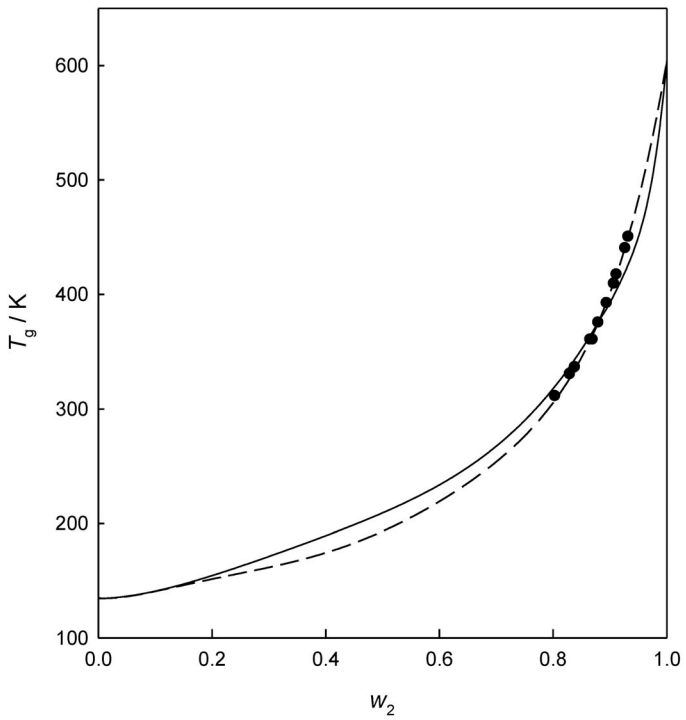

Fig. 6 Glass transition temperature vs. mass fraction of amylose in amylose–water solutions predicted by the AGCM (solid line) compared to the experimental data (●) [134] and the best CKM fit (dashed line).

© 2010, IUPAC

A few authors have attempted to use Kwei's equation (42) to describe T_g in water mixtures with food polymers [135–137], and in all cases it was tested in comparison with the GTM over a restricted range of water content ($w_1 < 0.3$). Because it has two adjustable parameters, the fitting of experimental data with the Kwei model seemed to be slightly more accurate than with the GTM within this restricted range of composition. However, an important shortcut of the Kwei model is that when $q \neq 0$, the T_g curve as a function of w_2 exhibits extreme behavior and an inflection point and must, therefore, always be S-shaped [138]. This is not the case with the GTM or the CKM, neither with the experimental T_g of aqueous cryoprotectants.

4.3 Maximally freeze-concentrated point

The empirical correlation proposed by Levine and Slade [4] for small carbohydrates and polyhydroxy compounds, based on the dependence of the maximally freeze-concentrated temperatures of $w_2 = 0.2$ solutions on the inverse of the solute molar mass, M_2, can be expressed as

$$T_g'/\mathrm{K} = 254 - 4263\, M_2^{-1} \tag{52}$$

The results are compared with the experimental data in Table 5, along with the estimations of the temperature and concentration of the maximally freeze-concentrated points obtained resorting to eqs. 48 and 49.

It is shown that the empirical correlation given by eq. 52 describes the experimental results reported by Levine and Slade [4] within ±2 K for mono- and disaccharides, but the discrepancies rise to ±(5–10) K for oligosaccharides.

The predictions of T_g' and C_g' using the Matveev and Ablett [76] model for the compounds listed in Table 5 are encouraging, taking into account that only the glass transition temperature and the associated heat capacity change of pure water and of the solute are required. In the case of mono- and disaccharides, it is also necessary to know their tautomeric composition.

It is noteworthy that the values of T_g' and C_g' reported by different authors for some compounds differ beyond the expected uncertainties. For instance, for glycerol, the values reported by Levine and Slade [4] and by Ablett et al. [86] are quite different and have been attributed to the fact that Levine and Slade have not used the SPD to calculate T_g', but a measured second transition in the DSC thermogram that other authors [86] consider to represent the onset of ice dissolution, occurring above T_g'.

Therefore, a new fit of all the available experimental T_g' values of polyhydroxy compounds as a function of the inverse of M_1 will be recommendable.

In the meantime, the Matveev and Ablett model or the extrapolation of the non-equilibrium freezing curve beyond the eutectic point to the intersection with the glass transition temperature could be used to obtain the maximally freeze-concentrated point with reasonably expected reliability.

© 2010, IUPAC

Table 5 Experimental and estimated maximally freeze-concentrated points for several polyhydroxy compounds.

Substance	T_g'/K Eq. 48	$100C_g'$ Eq. 49	T_g'/K Eq. 52	T_g'/K Exp.	$100C_g'$ Exp.	Ref.
Glycerol	177	80.4	207.7	208	54.0	4
				178	80.5	86
Ribose	213.5	81.1	225.6	226	67.1	4
				211	81.4	7
Sorbitol	217.6	80.7	230.6	229.5	81.3	4
				216	81.7	7
				230	81.3	140
Fructose	223	80.9	230.6	231	51.0	4
				220	82.5	7
				225	79.0	141
Glucose	232.7	77.0	230.6	230	70.9	4
				220	80.0	7
				230.6	74.7	140
Sucrose	241.7	74.0	241.5	241	64.1	4
				233	81.2	86
				232	81.7	7
Trehalose	–	–	241.5	243.5	83.3	4
				238	81.6	7
				250.8	81.2	92
Maltose	242	74.2	241.5	243.5	80.0	4
				236	81.6	7
				243.3	76.7	142
Maltotriose	254	67.8	245.5	249.5	69.0	4
				244	81.0	143
				249.5	75.0	144
Maltotetraose	256	74.4	247.6	253.5	64.5	4
				253.7	75.5	144
Maltohexaose	258	67.3	249.7	258.5	66.7	4
				258.5	75.0	145
Maltoheptaose	257	66.0	250.3	259.5	78.7	4
				255	78.0	143
Pullulan	260	72.8	–	263	74.0	143

5. MOLECULAR DYNAMICS SIMULATIONS OF THE GLASS TRANSITION

Molecular dynamics simulations (MD) provide an optimum level of detail for elucidating microscopic mechanisms, but also could help to estimate glass transition temperatures.

The reported simulations were carried out using either an isothermal-isobaric Monte Carlo algorithm (NPTMC) or an isothermal-isobaric molecular dynamics algorithm (NPTMD). The first determination of the glass transition temperature in glucose aqueous solutions by Caffarena and Grigera [146] used the change of the slope of the plot of the number of H-bonds vs. temperature, or the abrupt change in the water diffusion coefficient, to identify the glass transition temperature. These authors used a GROMOS (GROningen MOlecular Simulation) force field, where the interactions of the nonbonded atoms is represented with a 6–12 Lennard–Jones potential combined with coulombic interactions between atomic partial charges located on each of the C, O, and H atoms of the glucose, while the simple point charge (SPC/E) model was adopted for water.

© 2010, IUPAC

Conrad and de Pablo [147] used NPTMC to estimate the glass transition temperature of pure trehalose and trehalose aqueous solution ($w_2 = 0.8$) from the change in the slope of the system density as a function of temperature. The same criteria to determine T_g, but using NPTMD was reported for maltodecaose ($w_2 = 0.84$–0.99) aqueous solutions [148]; glucose and isomaltodecaose (in the pure form and hydrated with one molecule of water) [149]; pure cellulose [150]; pure myo- and neo-inositol [151]; pure glucose, sucrose, and trehalose [152]; trehalose ($w_2 = 0.95$–1.00) aqueous mixtures [153]; and glycerol [154].

Figure 7 shows the experimental and calculated T_g of concentrated aqueous trehalose solutions as a function of concentration on the very concentrated region ($w_2 > 0.92$) where MD simulations are available.

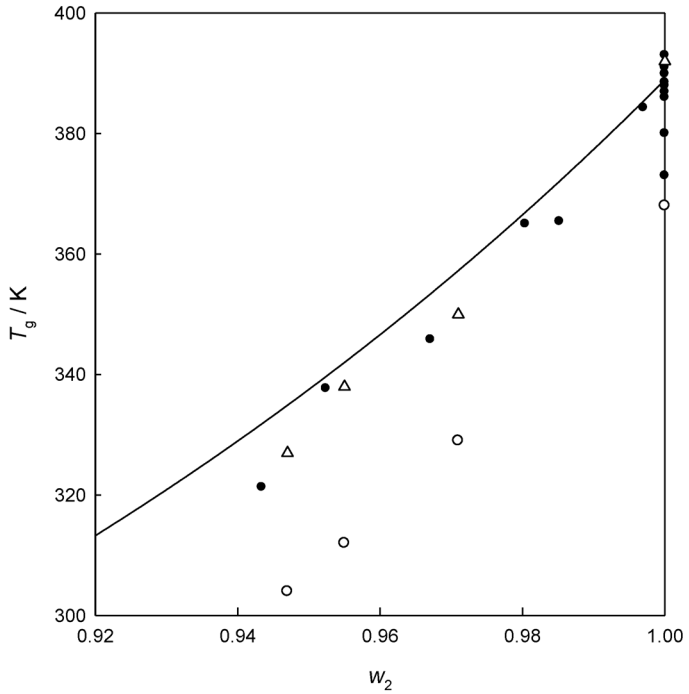

Fig. 7 Glass transition temperature vs. mass fraction of trehalose in concentrated trehalose aqueous solutions as predicted by NPTMD (△) [153], compared to experimental data (●) [7,92,123,126], (○) [152].

The effective cooling rate in the simulations is infinite, and the results are therefore not expected to agree with experimental values, but higher T_g is expected. The results shown in Fig. 7 for trehalose aqueous solutions seem to corroborate this assertion when the calculated T_g are compared with the experimental values measured by the same authors [153]. However, it is noteworthy that the simulated values are in good agreement with the T_g measured previously.

For glucose aqueous solutions, the simulated T_g values extend over the entire range of concentration, as shown in Fig. 8, and as expected they are 20–30 K higher than the experimental values.

The study of glassy molecular mixtures by MD has been hampered by the computational cost of atomistic simulations. Recently, a coarse grain molecular dynamics (CGMD) model for malto-oligosaccharides and their water mixtures have been developed [155,156] that is approximately 7000 times faster than atomistic MD. The coarse grain model for carbohydrates (denoted M3B), applied by Molinero et al. [156] for glucose, represents each glucose monomer by three beads while describing the water molecule as a single particle. The M3B model includes no charges or hydrogen-bonding terms,

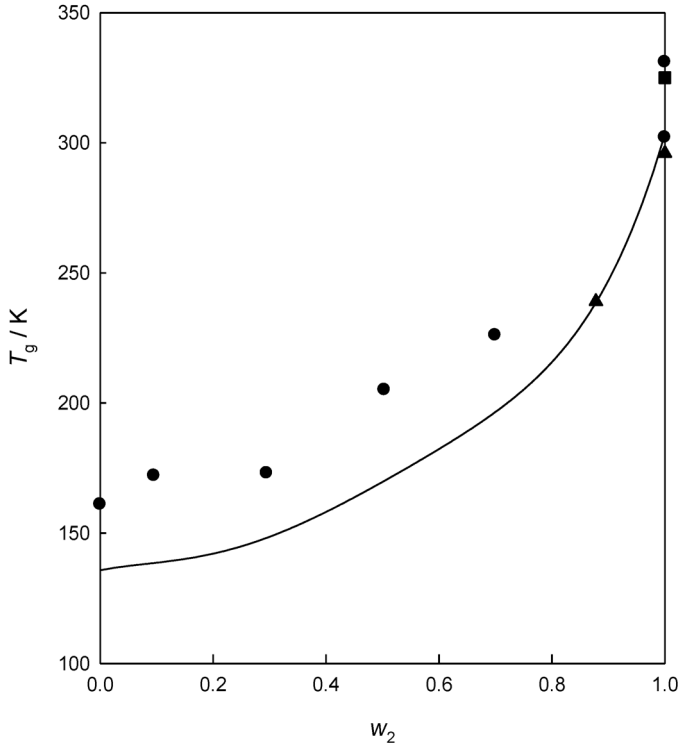

Fig. 8 Glass transition temperature of glucose vs. mass fraction of glucose in glucose aqueous solutions as predicted by MD (●) [146], NPTMD (■) [152], and CGMD (▲) [155], compared to experimental data (solid line) [157].

using only two-body Morse functions to describe long-range forces, and parameterized to fit the results from atomistic simulations for the gas phase and amorphous bulk phase of sugars over a wide range of pressures.

As it can be seen in Fig. 8, the M3B model leads to a T_g = 296 K for pure glucose, and a T_g = 239 K for w_2 = 0.88 glucose mixtures, in good agreement with the experiments.

A new application for MD studies of glassy materials lies in predicting the crystallizing propensity of systems interacting under systematically related potentials. These may be pair or many-body interactions, depending on the type of system of interest. The idea is to vary a single potential parameter and observe how the relation between melting point and glass temperature (here the temperature at which equilibrium is lost "ergodicity is broken") is affected. In the cases studied so far, the melting point has been affected much more strongly than is the simulation T_g, so that domains of easy glass-forming ability are revealed. The exploration of melting points of model systems, in relation to different liquid-state properties of interest by potential tuning, has been reported variously in the past [158,159], but the specific connection to glass-forming propensity has, surprisingly, not been one of them until the recent work of Molinero et al. [160].

The latter work has prompted interest in the possibility of finding cases where crystal melting points might be forced to such low values that not only the popular "2/3" rule* is discredited (revealed as a tautology) but T_m can even be shown to lie below T_g itself. Under the latter circumstances, a new

*The ratio of the glass transition temperature of the completely amorphous material to the melting temperature of the pure crystalline material, in Kelvin, is about 2/3.

© 2010, IUPAC

view of the glassy state (the "ideal glass-former" [161]) would emerge, as the understanding of crystallization kinetics would become irrelevant to the problem of understanding the existence of the glass transition. This could be regarded as an important research avenue. An interesting example is the case of the Gay–Berne model of liquid crystals, which can be generated by progressive elongation of the simple Lennard–Jones molecule in one direction. Such a study is currently being reported [162], and it appears that, near aspect ratios of 1.5, there is no crystalline form with a lower cohesive energy than that of the glass, in which case the glassy state, possessing also the entropy of disorder, must be the stable state of the system. Of course, it would require a large effort to create and eliminate all possible crystalline forms, but in simple systems like Gay–Berne there are not many options. The simulation approach is only feasible for pure materials, or compounds that melt congruently, since equilibration of solutions by diffusion is too slow a process to be followed. Melting of defect crystals needs no nucleation, hence can always be observed, even when re-solidification of the melt never happens.

It would be surprising if nature had not revealed some instances of this property, indeed it is possible that some sugar mixtures containing fructose as a component might reach this condition. An example from the ionic solutions literature, where the T_g appears to be above the melting point of any plausible crystal, is provided by Vuillard [163]. This is the case of the CrO_3 + H_2O system near the failed-crystal composition $H_2Cr_2O_7 \cdot 6H_2O$– as documented in Fig. 9.

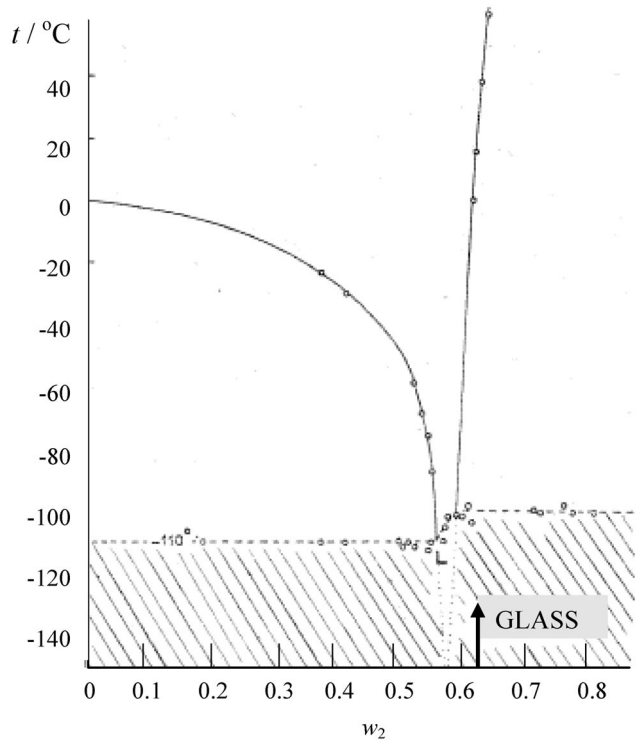

Fig. 9 Phase diagram of the system CrO_3 + H_2O, according to Vuillard [163], showing a hexahydrate compound at the composition indicated by the arrowhead. The CrO_3 + H_2O system has only the deep unrealized eutectic trough, terminated by the sloping line of glass transitions.

6. CONCLUSIONS AND OUTLOOK

Reliable estimations of the equilibrium ice-freezing and solute solubility curves of the SPD of aqueous solutions of simple carbohydrates can be obtained by resorting to UNIQUAC or UNIFAC group contribution models. Although there is a dearth of information on the effect of salts, it is believed that Pitzer's model could account for the effect of ionic solutes.

Regarding the prediction of the glass transition temperatures of aqueous solutions, the GTM and CKM require information on the volumetric or calorimetric properties of the pure solutes, which either are not available or exhibit a very large scatter (see Table 4). Because of the dependence of the glass transition temperatures determined by DSC in aqueous solutions with the heating rate, the number of heating cycles and the annealing time at low temperature, estimations of T_g within ±10 K could be considered satisfactory.

In the case of systems for which a few experimental values are available, even on a narrow range of composition, the use of eqs. 36 or 40 with k_{GT} (or k_{CK}) as an adjustable parameter is recommended for extrapolation purposes. When only the glass transition temperature of the pure solute, T_{g1}, is known, the empirical eq. 51 seems to be the best option.

The Matveev and Ablett model or the extrapolation of the non-equilibrium freezing curve beyond the eutectic point to the intersection with the glass transition temperature could be used to obtain the maximally freeze-concentrated point with reasonably expected reliability.

Molecular dynamics simulations can become an important theoretical tool for estimating glass transition temperatures in aqueous solutions, particularly when CGMD models of carbohydrates, instead of time-consuming atomistic simulations, can be proposed. Recent work by Angell and co-workers seems to indicate that MD could be also used to estimate the glass-forming propensity of liquid systems with related interaction potential and to help understand fundamental problems related to the behavior of non-equilibrium transitions, even in pure materials.

MEMBERSHIP OF SPONSORING BODIES

Membership of the IUPAC Physical and Biophysical Chemistry Division Committee for the period 2010–2011 is as follows:

***President*:** A. J. McQuillan (New Zealand); ***Vice President*:** K. Yamanouchi (Japan); ***Secretary*:** R. Marquardt (France); ***Past President*:** M. J. Rossi (Switzerland); ***Titular Members*:** J. H. Dymond (UK); A. Friedler (Israel); R. Guidelli (Italy); J.-G. Hou (China); B. D. Sykes (Canada); A. K. Wilson (USA); ***Associate Members*:** V. Barone (Italy); K. Bartik (Belgium); A. R. H. Goodwin (USA); V. Mišković-Stanković (Serbia); G. R. Moore (UK); M. Rico (Spain); ***National Representatives*:** K. Bhattacharyya (India); S.-J. Kim (Korea); V. Yu. Kukushkin (Russia); A. J. Mahmood (Bangladesh); O. V. Mamchenko (Ukraine); A. W. Mombrú Rodríguez (Uruguay); F. H. Quina (Brazil); N. Soon (Malaysia); V. Tsakova (Bulgaria); M. Witko (Poland).

Membership of the Task Group on Thermodynamics and Non-equilibrium Criteria for Development and Application of Supplemented Phase Diagrams was as follows:

***Chair*:** H. R. Corti (Argentina); ***Members*:** C. Austen Angell (USA); T. Auffret (UK); M. del Pilar Buera (Argentina); H. Levine (USA); D. S. Reid (USA); Y. Roos (Ireland); L. Slade (USA).

ACKNOWLEDGMENTS

H.R.C and M.P.B. thank CONICET, ANPCyT, and the University of Buenos Aires for financial support.

© 2010, IUPAC

REFERENCES

1. H. Levine, L. Slade. *Carbohydr. Polym*. **6**, 213 (1986).
2. H. Levine, L. Slade. *Water Science Reviews*, Vol. 3, pp. 79–185, Cambridge University Press, Cambridge (1987).
3. H. Levine, L. Slade. *Water and Food Quality*, pp. 71–134, Elsevier Applied Science, London (1988).
4. H. Levine, L. Slade. *J. Chem. Soc., Faraday Trans. 1* **84**, 2619 (1988).
5. L. Slade, H. Levine. *Pure Appl. Chem*. **60**, 1841 (1988).
6. Y. Roos, M. Karel. *Int. J. Food Sci. Technol.* **26**, 553 (1991).
7. Y. Roos. *Carbohydr. Res*. **238**, 39 (1993).
8. D. S. Reid. *Water Properties of Food, Pharmaceutical, and Biological Materials*, pp. 59–76, CRC, Taylor & Francis (2006).
9. R. A. Talja, Y. Roos. *Thermochim. Acta* **380**, 109 (2001).
10. K. S. Pitzer. *Thermodynamics*, 3rd ed., McGraw-Hill Series in Advanced Chemistry, Chap. 14, pp. 251, McGraw-Hill, New York (1995).
11. W. F. Giauque, J. W. Stout. *J. Am. Chem. Soc*. **58**, 1144 (1936).
12. C. A. Angell, M. Oguni, W. J. Sichina. *J. Phys. Chem*. **86**, 998 (1982).
13. R. J. Speedy. *J. Phys. Chem*. **91**, 3354 (1987).
14. R. J. Spencer, N. Møller, J. H. Weare. *Geochim. Cosmochim. Acta* **54**, 575 (1990).
15. J. M. Prausnitz, R. N. Lichtenhaler, E. G. de Azevedo. *Molecular Thermodynamics and Fluid-Phase Equilibria*, 2nd ed., Prentice Hall, New Jersey (1986).
16. S. A. Jónsdóttir, S. A. Cooke, E. A. Macedo. *Carbohydr. Res*. **337**, 1563 (2002).
17. M. Catté, C. G. Dussap, C. Achard, J. B. Gros. *Fluid Phase Equilib.* **96**, 33 (1994).
18. H. R. Corti. *Pure Appl. Chem*. **67**, 579 (1995).
19. D. S. Abrams, J. M. Prausnitz. *AIChE. J.* **21**, 116 (1975).
20. M. Le Maguer. *Physical Chemistry of Foods* (*IFT Basic Symposium Series 7*), pp. 1–45, Marcel Dekker, New York (1992).
21. B. L. Larsen, P. Rasmussen, A. Fredenslund. *Ind. Eng. Chem. Res*. **26**, 2274 (1987).
22. A. Bondi. *Physical Properties of Molecular Crystals, Liquids, and Glasses*, John Wiley, New York (1968).
23. A. M. Peres, E. A. Macedo. *Fluid Phase Equilib.* **123**, 71 (1996).
24. J. J. B. Machado, J. A. Coutinho, E. A. Macedo. *Fluid Phase Equilib.* **173**, 121 (2000).
25. A. Fredenslund, R. L. Jones, J. M. Prausnitz. *AIChE J.* **21**, 1086 (1975).
26. N. Gabas, C. Laguérie. *Bull. Soc. Chim. Fr*. **127**, 391 (1990).
27. Y. Abed, N. Gabas, M. L. Delia, T. Bounahmidi. *Fluid Phase Equilib.* **73**, 175 (1992).
28. C. Achard, J. B. Gros, C. G. Dussap. *Ind. Aliment. Agric.* **109**, 93 (1992).
29. M. Catté, C. G. Dussap, J. B. Gros. *Fluid Phase Equilib.* **105**, 1 (1995).
30. A. M. Peres, E. A. Macedo. *Fluid Phase Equilib.* **139**, 47 (1997).
31. H. Kuramochi, H. Noritomi, D. Hoshino, K. Nagahama. *Fluid Phase Equilib.* **130**, 117 (1997).
32. N. Spiliotis, D. Tassios. *Fluid Phase Equilib.* **173**, 39 (2000).
33. O. Ferreira, E. A. Brignole, E. A. Macedo. *Ind. Eng. Chem. Res.* **42**, 6212 (2003).
34. L. Ben Gaida, C. G. Dussap, J. B. Gros. *Food Chem*. **96**, 387 (2006).
35. W. G. McMillan, J. E. Mayer. *J. Chem. Phys*. **13**, 276 (1945).
36. K. S. Pitzer. "Ion interaction approach: Theory and data correlation", in *Activity Coefficients in Electrolyte Solutions*, R. M. Pytkowicz (Ed.), CRC Press, Boca Raton (1989).
37. R. A. Robinson, R. H. Stokes, K. N. Marsh. *J. Chem. Thermodyn.* **2**, 745 (1970).
38. T. M. Herrington, C. P. Meunier. *J. Chem. Soc., Faraday Trans. 1* **78**, 225 (1982).
39. H. L. Friedman, C. V. Krishnan. *J. Solution Chem*. **2**, 2460 (1973).
40. F. Franks, M. Pedley, D. S. Reid. *J. Chem. Soc., Faraday Trans. 1* **72**, 359 (1976).

© 2010, IUPAC

41. J. E. Desnoyers, G. Perron, L. Avédikian, J. P. Morel. *J. Solution Chem*. **5**, 631 (1976).
42. J. P. Morel, C. Lhermet. *Can. J. Chem*. **63**, 2639 (1985).
43. J. P. Morel, C. Lhermet, N. Morel-Desrosiers. *Can. J. Chem*. **64**, 996 (1986).
44. A. Maestre Alvarez, N. Morel-Desrosiers, J. P. Morel. *Can. J. Chem*. **65**, 2656 (1987).
45. J. P. Morel, C. Lhermet, N. Morel-Desrosiers. *J. Chem. Soc., Faraday Trans. 1* **84**, 2567 (1988).
46. N. Morel-Desrosiers, J. P. Morel. *J. Chem. Soc., Faraday Trans. 1* **85**, 3461 (1989).
47. N. Morel-Desrosiers, C. Lhermet, J. P. Morel. *J. Chem. Soc., Faraday Trans.* **87**, 2173 (1991).
48. N. Morel-Desrosiers, C. Lhermet, J. P. Morel. *J. Chem. Soc., Faraday Trans.* **89**, 1223 (1993).
49. P. Rongere, N. Morel-Desrosiers, J. P. Morel. *J. Chem. Soc., Faraday Trans.* **91**, 2771 (1995).
50. J. Wang, W. Liu, T. Bai, J. Lu. *J. Chem. Soc., Faraday Trans.* **89**, 1741 (1993).
51. J. Wang, L. Zeng, W. Liu, J. Lu. *Thermochim. Acta* **224**, 261 (1993).
52. J. Wang, W. Liu, J. Fan, J. Lu. *J. Chem. Soc., Faraday Trans.* **90**, 3281 (1994).
53. K. Zhuo, J. Wang, J. Zhou, J. Lu. *J. Phys. Chem. B* **101**, 3447 (1997).
54. K. Zhuo, J. Wang, J. Zhou, J. Lu. *J. Phys. Chem. B* **102**, 3574 (1998).
55. K. Zhuo, J. Wang, J. Zhou, Y. Gao, J. Lu. *Can. J. Chem. B* **77**, 232 (1999).
56. K. Zhuo, J. Wang, Y. Gao, J. Lu. *Carbohydr. Res*. **325**, 46 (2000).
57. Y. Jiang, S. Gao, S. Xia, J. Wang, K. Zhuo, M. Hu. *J. Chem. Thermodyn*. **34**, 1959 (2002).
58. Y. Jiang, M. Hu, P. Mu, J. Wang, K. Zhuo. *J. Chem. Eng. Data* **49**, 1418 (2004).
59. Y. Jiang, M. Hu, S. Li, J. Wang, K. Zhuo. *Carbohydr. Res*. **341**, 262 (2006).
60. K. Zhuo, G. Liu, Y. Wang, Q. Ren, J. Wang. *Fluid Phase Equilib.* **258**, 78 (2007).
61. K. Zhuo, H. Liu, H. Zhang, Y. Liu, J. Wang. *J. Chem. Thermodyn*. **40**, 889 (2008).
62. F. Hernández-Luis, E. Amado-Gonzalez, M. A. Esteso. *Carbohydr. Res*. **338**, 1415 (2003).
63. F. Hernández-Luis, D. Grandoso, M. Lemus. *J. Chem. Eng. Data* **49**, 668 (2004).
64. M. H. Cohen, D. Turnbull. *J. Chem. Phys.* **31**, 1164 (1959).
65. H. B. Callen. *Thermodynamics*, John Wiley, New York (1960).
66. J. M. Gordon, J. S. Taylor. *J. Appl. Chem*. **2**, 493 (1952).
67. R. Simha, R. F. Boyer. *J. Chem. Phys*. **37**, 1003 (1962).
68. E. Jenckel, R. Heusch. *Kolloidn. Zh*. **130**, 89 (1953).
69. A. V. Lesikar. *Phys. Chem. Glasses* **16**, 83 (1975).
70. P. R. Couchman, F. E. Karasz. *Macromolecules* **11**, 117 (1978).
71. P. R. Couchman. *Macromolecules* **20**, 1712 (1987).
72. J. M. Gordon, G. B. Rouse, J. H. Gibbs, W. M. Risen Jr. *J. Chem. Phys*. **66**, 4971 (1977).
73. G. ten Brinke, F. E. Karasz, T. S. Ellis. *Macromolecules* **16**, 244 (1983).
74. T. K. Kwei. *J. Polym. Sci., Polym. Lett. Ed*. **22**, 307 (1984).
75. Y. I. Matveev, V. Y. Grinberg, V. B. Tolstoguzov. *Food Hydrocolloids* **14**, 425 (2000).
76. Y. I. Matveev, S. Ablett. *Food Hydrocolloids* **16**, 419 (2002).
77. Y. I. Matveev. *Food Hydrocolloids* **18**, 363 (2004).
78. S. K. Chandrasekaran, C. J. King. *J. Food Sci*. **36**, 699 (1971).
79. R. N. Goldberg, Y. B. Tewari. *J. Phys. Chem. Ref. Data* **18**, 809 (1989).
80. F. E. Young. *J. Phys. Chem*. **61**, 616 (1957).
81. F. E. Young, F. T. Jones, A. J. Lewis. *J. Phys. Chem*. **56**, 1093 (1952).
82. F. E. Young, F. T. Jones. *J. Phys. Chem*. **53**, 1334 (1949).
83. G. Vavrinecz. *Z. Zuckerind*. **12**, 481 (1962).
84. A. N. Kanev, V. I. Kosyakov, D. V. Malakhov, E. Y. Shalaev. *Izv. Sib. Otd. Akad. Nauk SSSR. Ser. Khim. Nauk*. **2**, 11 (1989).
85. (a) Y. Roos, M. Karel. *CryoLett*. **12**, 367 (1991); (b) Y. Roos, M. Karel. *Biotechnol. Prog.* **6**, 159 (1990).
86. S. Ablett, M. J. Izzard, P. J. Lillford. *J. Chem. Soc., Faraday Trans*. **88**, 789 (1992).
87. *International Critical Tables*, McGraw-Hill, New York (1928).
88. F. W. Gayle, F. H. Cocks, M. L. Shepard. *J. Appl. Chem. Biotechnol*. **27**, 599 (1977).

© 2010, IUPAC

89. E. Y. Shalaev, F. Franks. *Thermochim. Acta* **255**, 49 (1995).
90. T. Chen, A. Fowler, M. Toner. *Cryobiology* **40**, 277 (2000).
91. H. Nicolajsen, A. Hvidt. *Cryobiology* **31**, 199 (1994).
92. D. P. Miller, J. J. de Pablo, H. R. Corti. *Pharm. Res*. **14**, 578 (1997).
93. P. M. Mehl. *J. Therm. Anal*. **49**, 817 (1997).
94. A. M. Lammert, S. J. Schmidt, G. A. Day. *Food Chem*. **61**, 139 (1998).
95. C. J. Roberts, F. Franks. *J. Chem. Soc., Faraday Trans*. **92**, 1337 (1998).
96. G. Blond, D. Simatos, M. Catté, C. G. Dussap, J. B. Gros. *Carbohydr. Res*. **298**, 139 (1997).
97. S. A. Jónsdóttir, P. Rasmussen. *Fluid Phase Equilib.* **158–160**, 411 (1999).
98. M. Sugisaki, H. Suga, S. Seki. *Bull. Chem. Soc. Jpn.* **41**, 2591 (1968).
99. D. R. MacFarlane, C. A. Angell. *J. Phys. Chem*. **88**, 759 (1984).
100. A. Hallbrucker, E. Mayer, G. P. Johari. *J. Phys. Chem*. **93**, 4986 (1989).
101. G. P. Johari, A. Hallbrucker, E. Mayer. *Science* **273**, 90 (1996).
102. G. P. Johari, A. Hallbrucker, E. Mayer. *Nature* **330**, 552 (1987).
103. A. Hallbrucker, E. Mayer, G. P. Johari. *Philos. Mag*. **60**, 170 (1989).
104. G. P. Johari, G. Astl, E. Mayer. *J. Chem. Phys*. **92**, 809 (1990).
105. G. P. Johari, A. Hallbrucker, E. Mayer. *J. Chem. Phys*. **92**, 6742 (1990).
106. I. Kohl, A. Hallbrucker, E. Mayer. *Phys. Chem. Chem. Phys.* **2**, 1579 (2000).
107. I. Kohl, L. Bachmann, E. Mayer, A. Hallbrucker, T. Loerting. *Nature* **435**, E1 (2005).
108. C. A. Angell, J. C. Tucker. *J. Phys. Chem*. **84**, 268 (1980).
109. M. Oguni, C. A. Angell. *J. Chem. Phys*. **73**, 1948 (1980).
110. K. Ito, C. T. Moynihan, C. A. Angell. *Nature* **398**, 492 (1999).
111. C. A. Angell. *Science* **319**, 582 (2008).
112. Y. Yue, C. A. Angell. *Nature* **427**, 717 (2004).
113. P. H. Poole, U. Essmann, F. Sciortino, H. E. Stanley. *Phys. Rev. E* **48**, 4605 (1993).
114. J. A. Schufle, M. Venugopalan. *J. Geophys. Res*. **72**, 3271 (1967).
115. B. V. Zheleznyi. *Russ. J. Phys. Chem*. **43**, 1311 (1969).
116. B. Luyet, D. Rasmussen. *Biodynamica* **10**, 167 (1968).
117. H. D. Goff. *Pure Appl. Chem*. **67**, 1801 (1995).
118. A. Saleki-Gerhardt, G. Zografi. *Pharm. Res*. **11**, 1166 (1994).
119. M.-A. Ottenhof, W. MacNaughtan, I. A. Farhat. *Carbohydr. Res*. **338**, 2195 (2003).
120. E. Y. Shalaev, F. Franks. *J. Chem. Soc., Faraday Trans.* **91**, 1511 (1995).
121. S. Shamblin, L. Taylor, G. Zografi, *J. Pharm. Sci*. **87**, 694 (1998).
122. A. A. Elamin, T. Sebhatu, C. Ahlneck. *Int. J. Pharm*. **119**, 25 (1995).
123. D. Miller, J. de Pablo. *J. Phys. Chem. B* **104**, 8876 (2000).
124. P. D. Orford, R. Parker, S. G. Ring. *Carbohydr. Res*. **196**, 11 (1990).
125. R. H. M. Hatley, C. Van den Berg, F. Franks. *Cryo-Lett.* **12**, 113 (1991).
126. D. P. Miller, J. J. de Pablo, H. R. Corti. *J. Phys. Chem. B* **103**, 10243 (1999).
127. L. M. Crowe, D. S. Reid, J. H. Crowe. *Biophys. J*. **71**, 2087 (1996).
128. M. E. Elias, A. M. Elias. *J. Mol. Liq*. **83**, 303 (1999).
129. S. P. Ding, J. Fan, J. L. Green, E. Sanchez, C. A. Angell. *J. Therm. Anal*. **47**, 1391 (1996).
130. L. Taylor, G. Zografi. *J. Pharm. Sci*. **87**, 1615 (1998).
131. P. D. Orford, R. Parker, S. G. Ring, A. C. Smith. *Int. J. Biol. Macromol.* **11**, 91 (1989).
132. I. I. Katkov, F. Levine. *Cryobiology* **49**, 62 (2004).
133. K. Kawai, T. S. Suzuki, R. Takai. *Cryo-Lett*. **23**, 79 (2002).
134. H. Bizot, P. Le Bail, B. Leroux, J. Davy, P. Roger, A. Buleon. *Carbohydr. Polym*. **32**, 33 (1997).
135. D. M. R. Georget, A. C. Smith, K. W. Waldron. *Thermochim. Acta* **332**, 203 (1999).
136. V. Micard, S. Guilbert. *Int. J. Biol. Macromol*. **27**, 229 (2000).
137. B. Cuq, C. Icard-Vernière. *J. Cereal Sci*. **33**, 213 (2001).
138. A. A. Lin, T. K. Kwei, A. Reiser. *Macromolecules* **22**, 4112 (1989).

139. P. J. A. Sobral, V. R. N. Telis, A. M. Q. B. Habitante, A. Sereno. *Thermochim. Acta* **376**, 83 (2001).
140. F. Franks. "Water and aqueous solutions: Recent advances", in *Properties of Water in Foods*, D. Simatos, J. L. Multon (Eds.), pp. 497–509, Martinus Nijhoff, Dordrecht (1985).
141. S. Ablett, A. H. Darke, M. J. Izzard, P. J. Lillford. *The Glassy State in Foods*, pp. 189–206, Nottingham Press, Leicestershire, UK (1993).
142. T. W. Schenz, K. Courtney, B. Israel. *Cryo-Lett.* **14**, 91 (1993).
143. S. Ablett, M. J. Izzard, P. J. Lillford, I. Arvanitoyannis, J. M. V. Blanshard. *Carbohydr. Res.* **246**, 13 (1993).
144. H. Kawai, M. Sakurai, Y. Inone, R. Chujo, S. Kobayashi. *Cryobiology* **29**, 599 (1992).
145. C. Van den Berg. *Carbohydr. Netherlands* **8**, 23 (1992).
146. E. R. Caffarena, J. R. Grigera. *Carbohydr. Res.* **300**, 51 (1997).
147. P. B. Conrad, J. J. de Pablo. *J. Phys. Chem. A* **103**, 4049 (1999).
148. F. A. Momany, J. L. Willett. *Biopolymers* **63**, 99 (2002).
149. S. Yoshioka, Y. Aso, S. Kojima. *Pharm. Res*. **20**, 873 (2003).
150. K. Mazeau, L. Heux. *J. Phys. Chem. B* **107**, 2394 (2003).
151. S. W. Watt, J. A. Chisholm, W. Jones, W. D. S. Motherwell. *J. Chem. Phys.* **121**, 9565 (2004).
152. A. Simperler, A. Kornherr, R. Chopra, P. A. Bonnet, W. Jones, W. D. S. Motherwell, G. Zifferer. *J. Phys. Chem. B* **110**, 19678 (2006).
153. A. Simperler, A. Kornherr, R. Chopra, W. Jones, W. D. S. Motherwell, G. Zifferer. *Carbohydr. Res*. **342**, 1470 (2007).
154. D. Li, B. Liu, Y. Liu, C. Chen. *Cryobiology* **56**, 114 (2008).
155. V. Molinero, W. A. J. Goddard III. *J. Phys. Chem. B* **108**, 1414 (2004).
156. V. Molinero, T. Çağin, W. A. Goddard III. *J. Phys. Chem. A* **108**, 3699 (2004).
157. Y. Roos. *Carbohydr. Res*. **300**, 51 (1997).
158. R. M. Lynden-Bell, P. G. Debenedetti. *J. Phys. Chem. B* **109**, 6527 (2005).
159. H. M. Gibson, N. B. Wilding. *Phys. Rev. E* **73**, 061507 (2006).
160. V. Molinero, S. Sastry, C. A. Angell. *Phys. Rev. Lett*. **97**, 075701 (2006).
161. C. A. Angell. *J. Non-Cryst. Solids* **354**, 4703 (2008).
162. V. Kapko, D. V. Matyushov, C. A. Angell. To be published.
163. G. Vuillard. *Ann. Chem.* **2**, 233 (1957).

Republication or reproduction of this report or its storage and/or dissemination by electronic means is permitted without the need for formal IUPAC permission on condition that an acknowledgment, with full reference to the source, along with use of the copyright symbol ©, the name IUPAC, and the year of publication, are prominently visible. Publication of a translation into another language is subject to the additional condition of prior approval from the relevant IUPAC National Adhering Organization.